The African Regional Greenhouse Gases Budget (2010-2019)

Yolandi Ernst[1], Sally Archibald[2], Frederic Chevallier[3], Philippe Ciais[3], Carlos Gonzalez Fischer[4], Benjamin Gaubert[5], Thomas Higginbottom[6], Steven Higgins[7], Shakirudeen Lawal[8], Fabrice Lacroix[9,10], Ronny Lauerwald[11], Mauro Lourenco[12,13], Carola Martens[14,15], Anteneh G. Mengistu[16], Lutz Merbold[17], Edward Mitchard[19], Mthokozisi Moyo[13], Hannah Nguyen[19], Michael O'Sullivan[20], Thais Rosan[21], Judith Rosentreter[22], Casey Ryan[7], Simon Scheiter[15], Stephen Sitch[21], Nicola Stevens[2,23], Torbern Tagesson[24,25], Hanqin Tian[26], Mengija Wang[27,28], Joel Woon[29], Bo Zheng[30,31], Yong Zhou[32,33], Robert J. Scholes[1]

[1] Global Change Institute, University of the Witwatersrand, Johannesburg, South Africa
[2] School of Animal, Plant and Environmental Sciences, University of the Witwatersrand, Johannesburg, Private Bag X3,WITS, 2050, South Africa
[3] Laboratoire des Sciences du Climat et de l'Environnement, LSCE/IPSL, CEA-CNRS-UVSQ, Université Paris-Saclay, Gif-sur-Yvette, France
[4] Department of Global Development, College of Agriculture and Life Sciences, Cornell University, Ithaca, NY, USA
[5] Atmospheric Chemistry Observations & Modeling Laboratory (ACOM), National Center for Atmospheric Research (NCAR), Boulder, CO
[6] School of GeoSciences, University of Edinburgh, Edinburgh, United Kingdom
[7] Plant Ecology, University of Bayreuth, Universitätsstraße 30, 95447 Bayreuth, Germany
[8] Department of Forestry and Environmental Resources, College of Natural Resources, North Carolina State University
[9] Climate and Environmental Physics, University of Bern, Bern, Switzerland
[10] Oeschger Centre for Climate Change Research (OCCR), University of Bern, Bern, Switzerland
[11] Université Paris-Saclay, INRAE, AgroParisTech, UMR ECOSYS, Palaiseau, France
[12] School of Geography, Archaeology and Environmental Studies, University of the Witwatersrand, South Africa.
[13] National Geographic Okavango Wilderness Project, Wild Bird Trust, South Africa
[14] Senckenberg Biodiversity and Climate Research Centre (SBiK-F), Senckenberganlage 25, 60325 Frankfurt am Main, Germany
[15] Institute of Physical Geography, Goethe University Frankfurt am Main, Altenhoeferallee 1, 60438 Frankfurt am Main, Germany
[16] Finnish Meteorological Institute, Helsinki, Finland
[17] Integrative Agroecology Group, Strategic Research Division Agroecology and Environment, Agroscope, Reckenholzstrsse 191, 8046 Zurich, Switzerland
[18] School of GeoSciences, King's Buildings, University of Edinburgh, Edinburgh EH9 3JN, UK
[19] Department of Geography, King's College London Strand, London WC2R 2LS, UK
[20] Faculty of Environment, Science and Economy, University of Exeter, Exeter EX4 4QF, UK
[21] College of Life and Environmental Sciences, University of Exeter, Exeter EX4 4RJ, UK
[22] Faculty of Science and Engineering, Southern Cross University, Lismore, NSW, Australia
[23] Environmental Change Institute, School of Geography and the Environment, University of Oxford, Oxford, UK
[24] Department of Physical Geography and Ecosystem Science, Lund University, Sölvegatan 12, SE-223 62 Lund, Sweden
[25] Department of Geosciences and Natural Resource Management, University of Copenhagen, Øster Voldgade 10, DK-1350 Copenhagen, Denmark

[26] School of Forestry and Wildlife Sciences, Auburn University, 602 Ducan Drive, Auburn, AL 36849, USA
[27] School of Geoscience and Technology, Zhengzhou University, 450001, China
[28] INRAE, UMR1391 ISPA, Universit´e de Bordeaux, F-33140 Villenave d'Ornon, France
[29] School of Environmental Sciences, University of Liverpool, Liverpool, UK
[30] Department of Earth System Science, Tsinghua University, Beijing 100084, China
[31] State Key Joint Laboratory of Environment Simulation and Pollution Control, School of Environment, Tsinghua University, Beijing 100084, China
[32] Department of Wildland Resources, Utah State University, Logan, Utah, 84321, USA
[33] Ecology Center, Utah State University, Logan, Utah, 84321, USA

Corresponding author(s):

Yolandi Ernst (yolandi.ernst@wits.ac.za)

Sally Archibald (sally.archibald@wits.ac.za)

Key Points:

1. Estimates for termite, herbivore and fire emissions from novel methods
2. Global woody biomass products constrained with high quality local data
3. Africa a net source (approximately carbon neutral) between 2010 and 2019, sink capacity decreasing

Abstract

As part of the REgional Carbon Cycle Assessment and Processes Phase 2 (RECCAP2) project, we developed a comprehensive African Greenhouse gases (GHG) budget for the period 2010-2019 and compared it to the budget over the 1985-2009 (RECCAP1) period. We considered bottom-up process-based models, data-driven remotely sensed products, and national GHG inventories in comparison with top-down atmospheric inversions, accounting also for lateral fluxes. We incorporated emission estimates derived from novel methodologies for termites, herbivores, and fire, which are particularly important in Africa. We further constrained global woody biomass change products with high-quality regional observations. During the RECCAP2 period, Africa's carbon sink capacity is decreasing, with net ecosystem exchange switching from a small sink of -0.61 ± 0.58 $PgCyr^{-1}$ in RECCAP1 to a small source in RECCAP2 at 0.162 (-1.793/2.633) $PgCyr^{-1}$. Net CO_2 emissions estimated from bottom-up approaches were 1.588 (-6.461/11.439) $PgCO_2yr^{-1}$, net CH_4 were 78.453 (36.665/59.677) $TgCH_4yr^{-1}$) and net N_2O were 1.81 (1.716/2.239) TgN_2Oyr^{-1}. Top-down atmospheric inversions showed similar trends. LUC emissions increased, representing one of the largest contributions at 1.746 (0.841/2.651) $PgCO_2eq\ yr^{-1}$ to

the African GHG budget and almost similar to emissions from fossil fuels at 1.743 (1.531/1.956) $PgCO_2eq\ yr^{-1}$, which also increased from RECCAP1. Additionally, wildfire emissions decreased, while fuelwood burning increased. For most component fluxes, uncertainty is large, highlighting the need for increased efforts to address Africa-specific data gaps. However, for RECCAP2, we improved our overall understanding of many of the important components of the African GHG budget that will assist to inform climate policy and action.

Plain Language Summary

We developed a comprehensive greenhouse gases (GHG) budget for Africa as part of the REgional Carbon Cycle Assessment and Processes Phase 2 (RECCAP2) project over the 2010-2019 period. We used global and local data sets and innovative methods to estimate the different components of the budget. Our estimates show that wildfire emissions decreased; termite emissions may be less than previously expected and emissions from large mammals are increasing. We also used data from new satellite technology to estimate carbon that is stored in above-ground biomass in Africa. With increasing land use change and fossil fuel usage in Africa, the net bottom-up GHG estimate shows Africa is a source at 5.518 (-2.666/12.859) $PgCO_2eq\ yr^{-1}$, with the top-down atmospheric inversion estimate smaller at 3.984 (3.126/4.849) $PgCO_2eq\ yr^{-1}$. However, our estimates continue to have large uncertainty owing to the differences between data sets and methods. It is therefore essential to increase efforts to expand on the availability of high quality local data. Nevertheless, our work improved our understanding of all the components of the African GHG budget and will help to inform climate policy and action.

1. Introduction

Africa's role in the global greenhouse gases (GHG) cycles is of great interest due both to the large landmass covered by the continent, and the potential for rapid change in coming decades as the human population increases and land use patterns continue to evolve. Africa contains some of the largest tracts of untransformed land in the world, although this is often heavily utilised for grazing, fuelwood and other natural resources. With a current population of about 1.4 billion, set to increase to over 2 billion by 2040 (United Nations Urban Settlement Programme, 2019), it is expected that large areas of land will be converted for agricultural production to feed this increasingly urbanised community and to increase country-level GDP. Concurrently there is massive interest in using African landscapes to store carbon and offset global carbon emissions (Armani et al., 2022). Quantifying the net effect of these competing trends on continental scale, improved carbon and GHG budgets is urgently needed.

Previous accounting efforts of the African GHG budget estimated the continent as a net biospheric sink but highlighted the large uncertainty associated with an inadequate observation network (Bombelli et al., 2009; Ciais et al., 2011; Valentini et al., 2014; Williams et al., 2007). Moreover, African savannas and woodlands, with seasonal rainfall, frequent fire and large populations of native and introduced herbivores, play a unique and significant role in the inter-annual variability of the continent's GHG fluxes that further contribute to uncertainty in estimates (Bombelli et al., 2009; Valentini et al., 2014).

Modeling studies indicate the risk for rapid and irreversible changes in vegetation cover in response to changing climates and CO_2 fertilisation (e.g. greening in northern ecosystems and browning in tropical biomes) (Winkler et al., 2021). Field observations further demonstrate both extensive woody thickening as well as areas of reduced productivity in recent years (Stevens et al., 2016). It is therefore imperative to develop reliable data on key carbon-cycle processes and GHG emissions. Since the last continental-scale GHG budget for the 1985-2009 period (Valentini et al., 2014), we have seen improved estimations of fire (Andela et al., 2017; Hantson et al., 2016; Lasslop et al., 2020) and herbivore emissions (Pachzelt et al., 2015) and better representation of African landscapes and functional types in Dynamic Global Vegetation Models (DGVMs) (e.g. aDGVM - Scheiter & Higgins, 2009). Estimates for other GHG budget components such as inland waters (Borges et al., 2022, 2015; Lauerwald et al., 2023) and geological fluxes (Etiope et al., 2019; Lacroix et al., 2020) are also better represented.

The current synthesis of the GHG budget of Africa aims to integrate the most contemporary modeling and observational datasets to present a comprehensive, up to date summary of the key sources and sinks of carbon, CO_2, CH_4 and N_2O greenhouse gases, and their associated uncertainties, from 2010 to 2019. Where possible, analyses that include the 1985-2009 period are presented for comparison. Due to the limitations imposed by the availability of some data sets, some estimates may represent alternative dates for the RECCAP1 (1985-2009) and RECCAP2 period (2010-2019) but reference periods are defined where necessary.

As part of the Regional Carbon Cycle Assessment and Processes Phase 2 (RECCAP2, https://www.globalcarbonproject.org/reccap/) initiative of the Global Carbon Project (GCP) (https://www.globalcarbonproject.org/index.htm), this paper will therefore address the policy-relevant objectives of RECCAP2 through a comprehensive overview of improved estimates of CO_2, CH_4 and N_2O fluxes and variability. In the following sections, we report the methodology and results for various component fluxes and uncertainties for Africa as a whole and for five ecoregions, delineated for interpretive purposes (Figure 1). Our synthesis generally follows the guidelines by (Ciais et al., 2022) for estimates derived from bottom-up approaches and those from top-down inversion models.

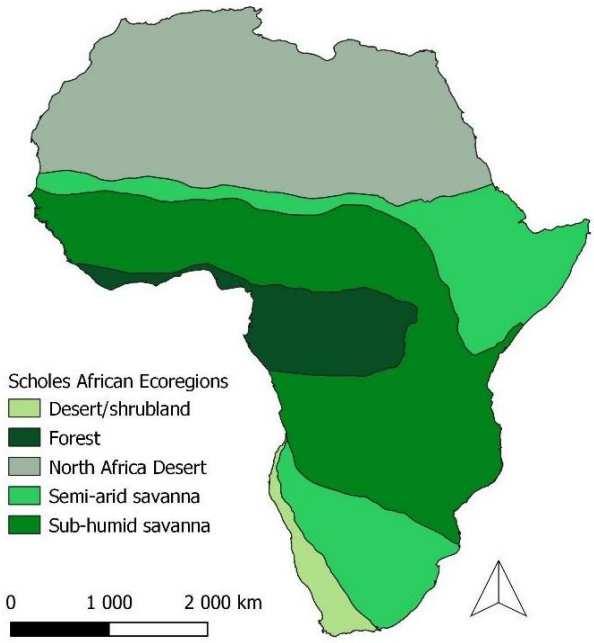

Figure 1. The Scholes African Ecoregions Map (Ernst and Scholes, 2023) was delineated by regrouping and smoothing the vegetation classification of the UNESCO/AETFAT/UNSO (White's) Vegetation Map of Africa (White, 1983) in accordance with the delineations of the distributions of Mean Annual Precipitation-determined ('stable') and Disturbance-determined ('unstable') savannas in Africa by (Sankaran et al., 2005).

2. African GHG component estimates

2.1. Land cover and land use change in Africa

Accurate quantification of baseline land cover area and its changes is essential for GHG flux and carbon stock accounting (Poulter et al., 2011). Estimating land cover and its changes is however associated with much uncertainty due to differences in data products and methodology, limited training and validation data,

and classification inconsistencies. Land cover estimates for 2009 and 2019 reported by the FAO, that include publicly available Global Land Cover (GLC) maps, MODIS land cover types based on the Land Cover Classification System, ESA-CCI annual land cover maps (Table 1) show a wide range of land cover area estimates for several categories (based on the land cover classification of the international standard system for Environmental and Economic Accounting Central Framework (SEEA CF)) and further indicate differences in trends between 2009 and 2019. For example, the MODIS based estimates of net increases or decreases indicate opposite trends for herbaceous crops, grassland, tree-covered areas, flooded vegetation and terrestrial barren land than for the ESA-CCI estimates (Table 1).

Table 1. Land cover area (Mha) for Africa calculated from publicly available Global Land Cover (GLC) maps, MODIS land cover types based on the Land Cover Classification System, LCCS (2001–2018) and the European Spatial Agency (ESA) Climate Change Initiative (CCI) annual land cover maps (1992–2018) as reported by the FAO (https://www.fao.org/faostat/en/#data/LC, accessed 14 October 2023).

	2009		2019			Change 2009-2019	
SEEC classes	**CCI-LC (Mha)**	**MODIS (Mha)**	**CCI-LC (Mha)**	**CGLS (Mha)**	**MODIS (Mha)**	**CCI-LC (Mha)**	**MODIS (Mha)**
Artificial surfaces	2.77	4.85	4.06	10.29	5.28	1.29	0.43
Herbaceous crops	358.26	145.52	357.14	236.34	145.83	-1.12	0.31
Woody crops	46.55		48.60			2.05	
Grassland	287.80	777.25	287.25	410.81	779.87	-0.55	2.61
Tree-covered areas	753.25	839.78	760.13	849.51	835.09	6.88	-4.70
Mangroves	3.76	4.00	3.72		3.80	-0.04	-0.20
Shrub-covered areas	460.65	196.51	454.20	434.63	195.38	-6.45	-1.13
Shrubs and/or herbaceous vegetation, aquatic or regularly flooded	26.07	4.38	25.97	21.21	4.89	-0.10	0.50
Sparsely natural vegetated areas	80.57		87.36			6.78	
Terrestrial barren land	951.70	997.61	942.86	997.68	1000.45	-8.84	2.84
Permanent snow and glaciers	0.07	0.00	0.07	0.00	0.02	0.00	0.02
Inland water bodies	31.00	30.31	31.11	23.60	30.12	0.11	-0.20

Recent advances in the quantification of land cover and land use is seeing a multitude of methodologies and modelling approaches that incorporate and harmonize satellite and inventory data sets in order to overcome some of the challenges (Ochiai et al., 2023). The Historic Land Dynamic Assessment + (HILDA+) model combines multiple open data sets including high-resolution remote sensing, reconstructions and statistics to assess changes in land use area extending from 1960 to 2019 at a 1km

spatial resolution (Winkler et al., 2021). Data from HILDA+, downloaded from https://landchangestories.org/hildaplus-mapviewer/ (accessed 14 October 2023), were used to calculate the area of the land use classes over the 1985 to 2019 period to illustrate how land use estimates have changed over time. Classes representing the natural landscapes such as Forest (Figure 2a), Sparse/no vegetation (Figure 2e) and Unmanaged grass/shrubland (Figure 2d) show an overall decrease in area over the 1985 to 2019 period. The decline in area were however slower during the last decade (2009-2019) than for the 1985 to 2008 period for both Forest and Sparse/no vegetation, while the area for Unmanaged grass/shrubland changed from decreasing to increasing during the last time period (Table 2). In contrast, the anthropogenic conversion of land is clearly evident from the increases in area for Cropland (Figure 2b), Pasture/rangeland (Figure 2c) and Urban expansion (Figure 2f) over the 1985 to 2019 period. Again, these increases in area occurred at a slower rate during the 2009 to 2019 period than during the 1985 to 2008 period (Table 2).

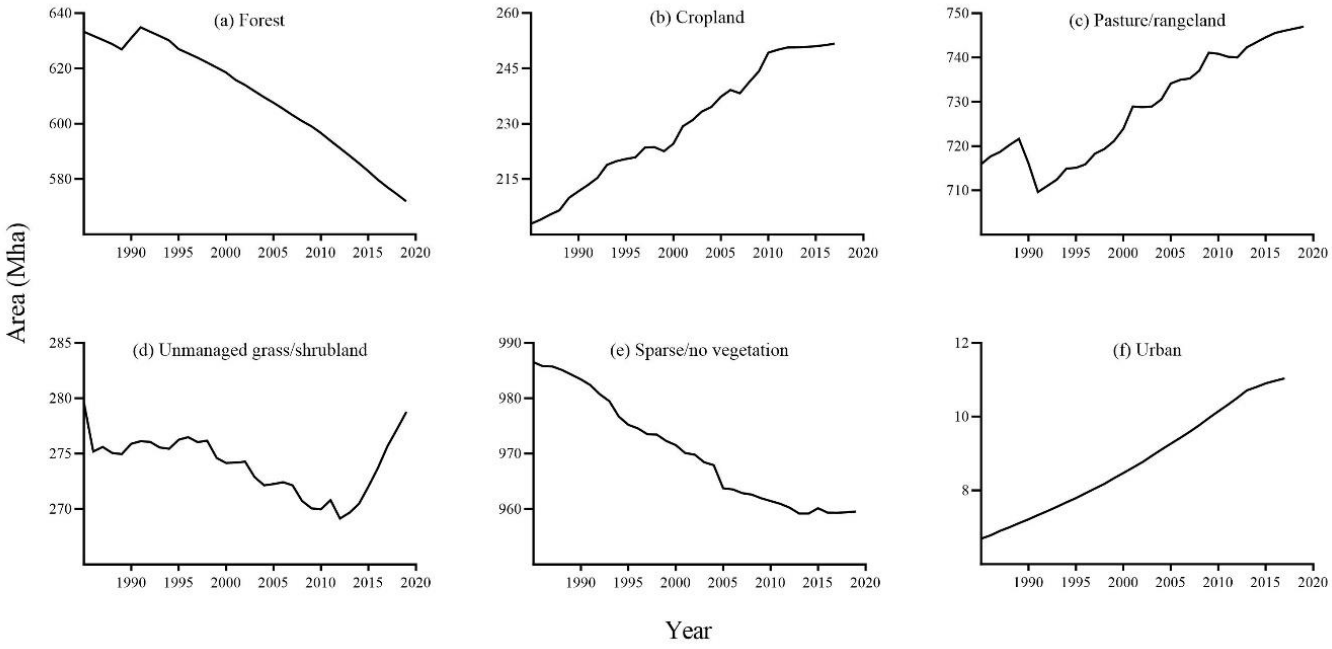

Figure 2. Change in LUC in the (a) Forest, (b) Cropland, (c) Pasture/rangeland, (d) Unmanaged grass/shrubland, (e) Sparse/no vegetation and (f) Urban LULC categories as estimated from the Hilda+ dataset. These classifications are not directly comparable to the Scholes Ecoregions as they represent land use rather than land cover.

Table 2. Estimated changes in land use area (Mha) from the HILDA+ modelled data set for the 1985 to 2008 and 2009 to 2019 periods.

	Net changes	
	1985-2008	**2009-2019**
Urban	2.93	1.45
Cropland	41.02	13.45
Pasture/rangeland	21.09	5.87
Forest	-32.24	-27.10
Unmanaged grass/shrubland	-8.90	8.71
Sparse/no vegetation	-23.90	-2.39

Forest loss estimated from the HILDA+ data were most dominant in the central African forest region for both periods (Figure 3). Indeed, Song et al., (2018) ascribes tree cover loss in the Congolian rainforest and Miombo woodlands in sub-Saharan Africa to agricultural practices, including a shift to commodity crop cultivation. Cropland expansion is observed across most of the continent but are most prominent in the western African and Sahel region south of the Sahara Desert when considering the HILDA+ data (Figure 3). These cropland patterns of change are largely similar to that of (Potapov et al., 2022) that produced a global cropland extent and change data set for the 2000 to 2019 time period based on the 30m spatial resolution Landsat satellite date archive. Although not directly comparable with the HILDA+ estimates, Potapov et al., (2022) additionally show large areas of cropland expansion in eastern Africa and report accelerated rates of cropland increase since 2004. Beside cropland expansion in the Sahel region, increases in short vegetation on bare ground due to extreme rainfall anomalies explain the greening of the Sahel region (Song et al., 2018). This greening inclination - through increased rainfall and CO_2 fertilisation - further affects the savanna regions in Central and West Africa through gross increases in woody cover (including forest expansion and woody encroachment) (Song et al., 2018).

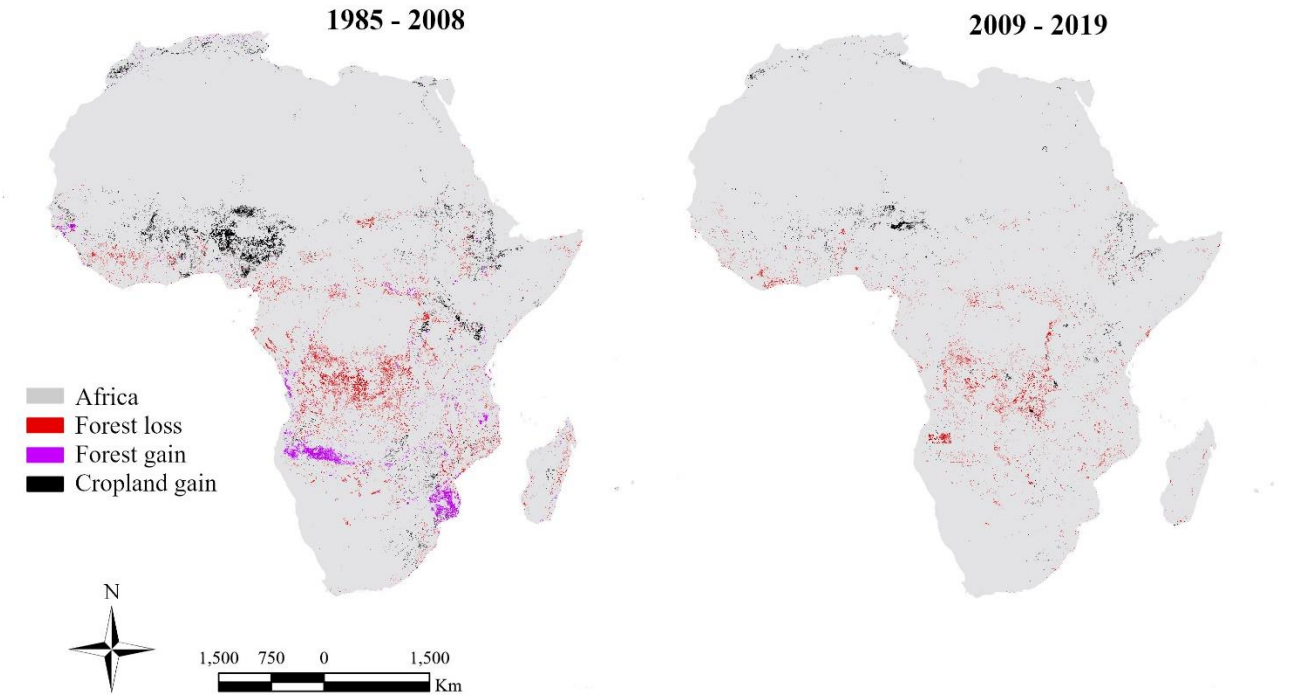

Figure 3. Maps of the extent of forest loss (red), forest gain (purple) and cropland gain (black) across Africa estimated from the HILDA+ modelled land use data set for the 1985-2008 and 2009-2019 time periods.

2.2. Biomass

2.2.1. Aboveground biomass change

A highly dynamic aboveground biomass (AGB) stock is the norm for many ecosystems in Africa, where natural and human disturbances are common, but recovery rates are also rapid (Syampungani et al., 2016). This complicates assessments of degradation and AGB trends (McNicol et al., 2018). For RECCAP1, Valentini et al., (2014) estimated emissions from LULCC in Africa that were equivalent to fossil fuel emissions based on a bookkeeping model, while field observations showed increases in woody biomass across intact African tropical forests (Lewis et al., 2009). The net effect of these generated a small sink. Since the RECCAP1 period, novel L-VOD passive microwave data (Diouf et al., 2015) and LiDAR-based biomass data (Potapov et al., 2021) have become available. These data have the potential to provide more comprehensive information on AGB changes than estimates derived from changes in land cover as they measure AGB change within the land cover classes. They therefore account both for losses due to degradation, natural disturbance as well as gains from regrowing vegetation and environmental drivers such

as CO_2-fertilisation. These within-land cover changes are important for Africa as land cover conversion is estimated to account for only about 25% of the AGB change on the continent (Feng et al., 2021; McNicol et al., 2018). However, although many papers reporting changes in AGB in Africa have been published within the 1985-2019 period, there is no agreement on the regional trends or magnitude of the changes.

(Baccini et al., 2017) reported widespread biomass losses in Africa of approximately -72 ± 32 $TgCyr^{-1}$ for the period 2003-2014. These are slightly lower than most previous estimates (ranging from -72 to -234 $TgCyr^{-1}$) but similar to the losses of -100 $TgCyr^{-1}$ reported by (Brandt et al., 2018) from 2010-2016 using L-VOD passive microwave data. However, other studies find that gains outweigh losses: (Zhao et al., 2022) report net increases in AGB of 15.7 ± 3.3 $TgCyr^{-1}$ between 2010 and 2019 in central African forests and savannas despite large scale losses in the Democratic Republic of Congo, and McNicol et al., (2018) found no significant trend in AGB in southern Africa over the 2007-2010 period (-20 ± 40 $TgCyr^{-1}$). Liu et al., (2015) showed losses of <10 $TgCyr^{-1}$ for tropical African forests, which were more than offset by increases in savannas and woodlands over the 1993-2012 period. Pelletier et al., (2018) demonstrated that biomass growth rates in field plots in Zambia were higher than nationally reported losses due to LUC. These disagreements in AGB change estimates are largely due to the varied methods used, which include bookkeeping models, LiDAR-derived products, and various microwave-derived products. However, differences in the observation time periods might also add to the uncertainty due to large inter-annual variation in AGB.

For RECCAP2, we compared five microwave- and VOD-derived AGB change estimates from 2010 to 2017, three of which have been developed and calibrated specifically for Africa. The L-VOD product (Brandt et al., 2018) was calibrated against the Baccini et al., (2012) LIDAR-derived AGB. The X-VOD product (Wang et al., 2021) was retrieved from the AMSR2/AMSR-E brightness temperature observations at X-band, with Saatchi et al., (2011) AGB (LiDAR-derived), (Bouvet et al., 2018) AGB (SAR-derived), GlobBiomass (SAR-derived AGB) and ESA-CCI AGB (SAR-derived AGB) as the calibration references. The National Centre for Earth Observation (NCEO) product (Rodríguez-Veiga et al., 2017) uses GEDI canopy-height data and L-band SAR to produce a canopy-height model calibrated against LiDAR-derived biomass data. The global ESA-CCI Biomass product (Santoro et al., 2021) uses both C- and L-band RADAR to estimate growing stock volume, and converts this to AGB using allometric equations from published wood density and biomass expansion data. The updated McNicol et al., (2018) product for southern Africa is focused on accurately estimating change in non-forest African ecosystems (i.e. in contrast to L-VOD which is also sensitive to high-biomass regions), and trains its product with in-situ biomass measurements. All products have potential artifacts from soil moisture and

range in spatial resolution from 25 km (Brandt LVOD) to 25 m (McNicol product). More details on the products are available in Table S1.

For each product, we calculated annual change as (AGB_{2017}-AGB_{2010})/7. As 2017 was the end of a severe multi-year drought in southern Africa (Blamey et al., 2018) the trends might not be reliable, but it is the first time that so many different products have been compared over the same period and regions.

All the products estimate net AGB losses at the scale of Africa, ranging from -71.9 to -309.9 $TgCyr^{-1}$, but there was no consistency in predicted trends across biome classes or regions (Table 3, Figure 4). For example the ESA-CCI biomass product predicted biomass gains of 44 $TgCyr^{-1}$ in forest but losses of -118 $TCyr^{-1}$ in sub-humid savannas, and the Brandt L-VOD product showed the opposite trend (forest loss: -20.8 $TgCyr^{-1}$, sub-humid savanna gains: 36.6 $TgCyr^{-1}$). Generally these estimates are within the range reported by Valentini et al., (2014), but the uncertainty remains high for RECCAP2. Global RADAR and VOD products are currently unlikely to represent the dynamics of African woodlands accurately because they often lack African calibration data, and potentially require locally defined algorithms to represent the lower-biomass dynamic of African woodlands.

Table 3: Estimated net aboveground biomass (AGB) annual change 2010-2017 (in $TgCyr^{-1}$) for Africa and its ecoregions.

	1985-2009		**2010-2019**			
Region	**Valentini et al. (2014)**	**CCI**	**NCEO**	**L-VOD (Brand et al. 2018)**	**X-VOD Wang et al 2021**	**McNicol et al. (2018)**
NH Desert		0.1	-1.4	-5.9	-3.0	
Forest		44.8	-80.2	-20.8	-147.4	
Sub-humid savanna		-118.6	-63.0	36.2	-92.1	
Semi-arid savanna		-17.9	-7.5	-71.3	-62.6	
Desert/shrubland		-0.3	-0.2	-10.0	-4.8	
Miombo Ecoregion		-98.0	-22.0	-1.0	17.0	3.6
Africa	**-234 to -72**	**-92**	**-152.3**	**-71.9**	**-309.9**	

Note. Positive values represent fluxes into the land surface, and negative values fluxes out to the atmosphere. Products ordered from global (left) to regional (right) calibrations. The Miombo Ecoregion was added to include the locally-calibrated and developed (McNicol et al., 2018) product and because it is a region of rapid change.

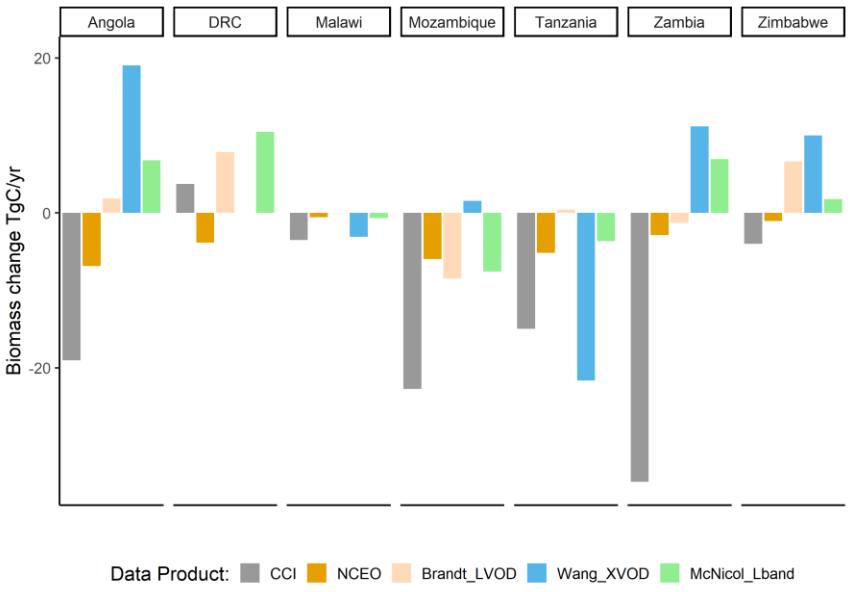

Figure 4: Change in aboveground biomass across seven countries in southern Africa for the period 2010-2017 as reported by five different RADAR-derived data products. Positive values represent fluxes into the land surface (sink), and negative values fluxes out to the atmosphere (source). There is no clarity on the trends between or within countries, but regionally and locally calibrated products report more sink capacity than globally calibrated products overall.

2.2.2. Belowground carbon and biomass

Since the previous synthesis of the African GHG budget, soil organic carbon (SOC) estimates (Table 4) have improved with the ISRIC (International Soil Reference and Information Centre) producing soil property maps for the continent at 250 m resolution (Hengl et al., 2015, 2017). These SoilGrids (https://www.isric.org/explore/soilgrids, accessed 14 October 2023) are interpolated from a network of several thousand soil cores and several hundred thousand surface samples, and estimate SOC of Africa to be 87.7 PgC. However, these maps still do not accurately map or account for peatlands, which are estimated to contain significant stores of carbon and are also being degraded at approximately 0.013 $PgCyr^{-1}$ (Joosten, 2009). Currently peat stocks are estimated at 36.9 PgC (UNEP, 2022), which is ~ 3 times higher than previous estimates of ~11 PgC due to new reserves found in the Congo basin (Dargie et al., 2017), and novel peat mapping methods (Lourenco et al., 2022). Peat loss is estimated to be ~0.0124 $PgCyr^{-1}$ (Joosten, 2009) and is increasing.

Below-ground biomass carbon estimates can vary substantially between ecosystems (Mokany et al., 2006). Stocks in grasslands and savannas are more variable and more difficult to generalize from above-ground stocks than in woodlands and forests but grasslands can contain equivalently high below-ground biomass stores to adjacent woodlands (Gomes et al., 2021), which is not accurately represented in any existing continental-scale studies, and the current below-ground biomass values are likely under-estimates.

Below-ground stocks modeled from DGVMs vary greatly ranging from 87.48 to 259.53 PgC in the previous RECCAP period (Valentini et al., 2014). For the RECCAP2 period, aDGVM, a dynamic vegetation model developed for African ecosystems (Scheiter & Higgins, 2009, see also section 2.3.3) estimates total stocks to be 98.85 PgC, of which SOC is 76.77 Pg and belowground biomass carbon 22.08 Pg. The Trendy models show a mean SOC of 148 ± 60 Pg and all but three show an increasing trend.

Table 4: Soil Organic Carbon, peat carbon stocks and estimated peat loss rates for Africa per ecoregion.

	SOC (Pg) from SoilGrids	**Peat Carbon (Pg)**				**Valentini et al. 2014**	**2009-2019**		
	Total	1990[a]	2008[a]	2020[b]	Loss rate ($PgCyr^{-1}$)	Total below-ground C	aDGVM # SOC	aDGVM biomass C	aDGVM Total belowground C
NA Desert	3.7		2.1				4.33	0.67	5
Forest	15.7		3.6				13.29	3.92	17.21
Desert/shrubland	1.0		0.0				1.03	0.15	1.18
Sub-humid savanna	46.9		4.0				40.98	12.91	53.89
Semi-arid savanna	20.3		1.1				17.15	4.42	21.57
Total	**87.7**	**11.0**	**10.78**	**36.9**	**0.013**	**167 (87-259)**	**76.77**	**22.08**	**98.85**

*Valentini et al., (2014) model average - including biomass carbon
#aDGVM is a dynamic vegetation model developed for African ecosystems, see section 2.3.3
[a] Joosten (2009)
[b] UNEP – including new reserves in the Congo

2.3. Gross and Net primary production estimates

2.3.1. Satellite observation constrained GPP models

We used seven Earth observation based global scale vegetation gross primary productivity (GPP) data sets collected by (Tagesson et al., 2021) for estimating Africa's GPP budgets 1982-2015. The

contribution of Africa to the mean, trend and inter-annual variability in the global scale GPP were estimated following Ahlström et al., (2015). The products with their spatial and temporal resolution and estimates are listed in Table S2 and described in Tagesson et al., (2017). The average GPP budget for Africa 1982-2015 was 23.39 ± 0.52 (± one standard deviation of inter-annual variability) ± 2.45 PgC yr^{-1} (± one standard deviation of model variability) (Table S2), which represents about 20% of the annual global GPP. This is relatively close to the 22.3% share Africa has to the global terrestrial surface area. Satellite observations indicate that the GPP is increasing by 39.7 ± 6.8 ± 37.4 TgC yr^{-1}, over the 1982-2015 period (about 18.2% of the global trend) but the share of Africa to the inter-annual variability in the global GPP budgets was relatively low (7.2 ± 1.3 ± 4.0 %).

Sub-humid savannas and forests were the main contributors to African GPP, contributing with more than 50% and ~25%, respectively (Table 5). Sub-humid savannas drove both the increasing trends and the inter-annual variability in GPP, but the forest GPP showed less strong trends, indicating relatively stable vegetation conditions compared to the other ecoregions. Instead, semi-arid savanna, which contributed relatively little (3.72 ± 0.15 ± 0.31 PgCyr^{-1}) to the mean African GPP budgets, contributed substantially to the GPP trends (about a quarter of the GPP increases occurred in semi-arid savannas). Semi-arid regions in Africa are steadily becoming encroached with woody vegetation (Venter et al., 2018) and are important in terms of their inter-annual variability (Ahlström et al., 2015). The NH Desert and Desert/Shrubland regions have a very low share (about 1%) to the African GPP budget (Table 5). However, significant NA Desert trends and inter-annual variability (Table 5) indicate considerable changes in the vegetation cover during recent decades likely driven by CO_2 fertilisation (Song et al., 2018).

The GPP of Africa increased over the period 1982-2015; both according to the trend and the differences in the mean GPP budgets between the long-term averages of the 1985-2009 and 2009-2015 periods (Table 5). However, the GPP trends switched from being positive to negative for most land cover classes between the two periods (Table 5). This could be caused by the strong drought at the end of the study period in 2015 (Brandt et al., 2018). Other reasons for a slowing down of the GPP trends could be a decrease in the degree to which CO_2 is upregulating photosynthesis (fertilisation effect) (Wang et al., 2020), enhanced constraints from water supply, nutrient limitation, and land cover change (Feng et al., 2021; Peñuelas et al., 2013; Piao et al., 2020; Yuan et al., 2019). Trends in the 2009-2015 period should be used with caution since the data on GPP trends cover only six years. Still, Africa's contribution to the global GPP budgets are similar for both study periods. Forests show a minor decrease in their contribution to the GPP budgets between RECCAP1 and RECCAP2, with increases in semi-arid savanna compensating for this. The semi-arid savanna also has a large GPP trend between1982-2015 compared to forests, explaining their larger share during the RECCAP2 period.

Table 5. The GPP mean, trend and inter-annual variability (± one standard deviation of inter-annual variability ± model variability) from seven global earth observation products for Africa and its ecoregions for the 1985-2009 and 2009-2015 periods.

Region	Period	Mean GPP ($PgCyr^{-1}$)	Trend GPP ($TgCyr^{-2}$)	Contributions (%) of Africa to global GPP budget/ Ecoregions to Africa GPP budget		
				Mean	IAV*	Trend *
Africa (22.3% of global surface)	1985-2009	23.45 ± 0.40 ± 2.49	42.2 ± 7.25 ± 43.45	20.2 ± 0.3 ± 1.8	7.5 ± 1.1 ± 6.4	24.3 ± 4.2 ± 14.0
	2009-2015	24.67 ± 0.30 ± 2.46	-31.6 ± 60.92 ± 38.57	20.5 ± 0.3 ± 1.5	37.1 ± 3.5 ± 7.0	4.9 ± 9.4 ± 9.5
NA Desert (34.7% of Africa)	1985-2009	0.31 ± 0.02 ± 0.13	1.08 ± 0.52 ± 1.22	1.28 ± 0.1 ± 0.6	6.1 ± 0.4 ± 2.7	2.6 ± 1.3 ± 6.3
	2009-2015	0.38 ± 0.02 ± 0.12	-6.20 ± 1.52 ± 4.17	1.48 ± 0.1 ± 0.4	1.0 ± 0.2 ± 2.3	17.0 ± 4.3 ± 10.5
Forests (8.2% of Africa)	1985-2009	5.99 ± 0.06 ± 0.49	6.07 ± 1.05 ± 10.49	24.7 ± 0.2 ± 4.0	34.2 ± 1.1 ± 7.9	14.4 ± 2.5 ± 22.5
	2009-2015	5.76 ± 0.07 ± 0.47	-21.32 ± 10.1 ± 9.66	22.6 ± 0.3 ± 4.0	12.7 ± 1.6 ± 9.2	59.7 ± 28.3 ± 6.8
Desert/ Shrubland (2.4% of Africa)	1985-2009	0.13 ± 0.01 ± 0.06	0.52 ± 0.18 ± 0.41	0.5 ± 0.3 ± 0.28	4.3 ± 0.1 ± 1.4	1.2 ± 0.4 ± 0.6
	2009-2015	0.15 ± 0.3 ± 0.06	-0.02 ± 2.88 ± 1.27	0.6 ± 0.1 ± 0.3	1.1 ± 0.2 ± 1.6	0.0 ± 8.1 ± 3.1
Sub-humid savanna (34.0% of Africa)	1985-2009	13.14 ± 0.22 ± 2.39	22.96 ± 4.09 ± 25.21	54.2 ± 0.9 ± 4.5	50.5 ± 3.9 ± 7.9	54.5 ± 9.7 ± 21.9
	2009-2015	13.95 ± 0.16 ± 2.33	-5.13 ± 32.85 ± 29.28	54.8 ± 0.6 ± 4.1	67.0 ± 3.3 ± 9.9	14.4 ± 92.0 ± 22.0
Semi-arid savanna (20.7% of Africa)	1985-2009	3.72 ± 0.15 ± 0.31	11.52 ± 3.49 ± 7.80	13.1 ± 0.6 ± 0.2	4.9 ± 2.2 ± 12.4	27.3 ± 8.3 ± 13.0
	2009-2015	3.71 ± 0.14 ± 0.60	3.06 ± 29.76 ± 14.59	14.6 ± 0.6 ± 1.3	18.2 ± 2.0 ± 15.2	8.6 ± 83.3 ± 13.4

*Trends and IAV in the RECCAP2 period should be used cautiously because of the short study period, but is still included for consistency.

2.3.2. Ecosystem model ensembles including LULCC: Trends in the Land Carbon Fluxes (TRENDY)

Outputs from an ensemble of 14 Dynamic Global Vegetation Models (DGVMs) from the TRENDY v.9 model suite were forced with observed changes in climate, CO_2 and nitrogen deposition, and LULCC (Land Use Land Cover Change HYDE3.2 within LUH2-GCB) over the period 1985 to 2019 (Friedlingstein et al., 2020) (Table 6).

We estimated changes in the African regional carbon fluxes and sinks and calculated the attribution to the underlying environmental drivers and the different ecoregions (Figure 5). Between 2000 and 2019 there were widespread but subtle losses due to climate change and variability (Figure 5c). The models also show a strong tropical forest uptake response driven by enhanced atmospheric CO_2 concentrations (Figure 5b) while LULCC losses were concentrated in East and West Africa (Figure 5d). These large opposing fluxes result in Africa acting as a net sink between 2000 and 2019 (Figure 5a), but there are still large uncertainties around the magnitude of the estimates.

The model ensemble show that losses due to LULCC in Africa have increased over time (from 0.18 to 0.46 $PgCyr^{-1}$ at a similar rate but in the opposite direction than the CO_2 fertilisation sink increase (from -0.41 to -0.55 $PgCyr^{-1}$, Table 6). Climate-induced losses have decreased to almost zero (Table 6) likely due to the breaking of the decades-long drought in the Sahel. Consequently the biospheric sink capacity in Africa has increased to -0.09 ± 0.24 $PgCyr^{-1}$ in the last decade. The LUC fluxes are spatially concentrated in the sub-humid savanna (a net source of 0.04 ± 0.17 $PgCyr^{-1}$), while most of the sink capacity is concentrated in the tropical forests (-0.08 ± 0.06 $PgCyr^{-1}$). This estimated sink capacity is an order of magnitude lower than that estimated from models that do not include land use and land cover: Africa NEE (including fire disturbances) estimated by Trendy model ensembles was -0.09 ± 0.24 $PgCyr^{-1}$ in 2010-2019 compared with -2.21 $PgCyr^{-1}$ for aDGVM – section 2.3.3).

We find large gross changes in the vegetation stocks but the net carbon stocks remain the same (Figure 6). Soil carbon pools are increasing: i.e. the DGVM models predict that the increase in CO_2 uptake caused by CO_2 fertilisation continues to be larger than fluxes to the atmosphere due to increased microbial respiration rates, LULCC and climate change.

Table 6. Regional carbon fluxes ($PgCyr^{-1}$) decomposed into the three main drivers; climate change (CLIM), CO_2 fertilisation (CO_2), and land use land cover change (LULCC) over the last four decades. Positive values represent fluxes out (source) of the biosphere and negative values, fluxes in (sinks).

Region	**Forcing**	**Net Ecosystem Exchange (NEE $PgCyr^{-1}$)**			
		1980s	1990s	2000s	2010s
Africa	CLIM	0.33 ± 0.21	0.16 ± 0.12	0.21 ± 0.13	0.00 ± 0.15
	CO_2	-0.41 ± 0.17	-0.39 ± 0.18	-0.56 ± 0.21	-0.55 ± 0.24
	LULCC	0.18 ± 0.12	0.22 ± 0.13	0.28 ± 0.1	0.46 ± 0.15
	NET	0.10 ± 0.19	-0.01 ± 0.20	-0.07 ± 0.21	-0.09 ± 0.24
North Africa Desert	CLIM	0.01 ± 0.02	-0.00 ± 0.01	0.01 ± 0.00	-0.00 ± 0.02
	CO_2	-0.01 ± 0.01	-0.01 ± 0.00	-0.01 ± 0.01	-0.01 ± 0.01
	LULCC	-0.00 ± 0.01	-0.00 ± 0.01	-0.00 ± 0.01	-0.00 ± 0.01
	NET	0.01 ± 0.01	-0.00 ± 0.01	-0.01 ± 0.01	-0.01 ± 0.02
Forest	CLIM	0.03 ± 0.03	0.02 ± 0.03	0.03 ± 0.03	0.02 ± 0.02
	CO_2	-0.11 ± 0.04	-0.13 ± 0.05	-0.15 ± 0.05	-0.17 ± 0.07
	LULCC	0.04 ± 0.02	0.05 ± 0.03	0.05 ± 0.03	0.07 ± 0.04
	NET	-0.04 ± 0.04	-0.06 ± 0.05	-0.07 ± 0.04	-0.08 ± 0.06
Sub-humid savanna	CLIM	0.18 ± 0.14	0.11 ± 0.09	0.13 ± 0.09	0.01 ± 0.08
	CO_2	-0.22 ± 0.13	-0.21 ± 0.13	-0.30 ± 0.17	-0.30 ± 0.17
	LULCC	0.12 ± 0.08	0.15 ± 0.08	0.20 ± 0.07	0.33 ± 0.12
	NET	0.09 ± 0.13	0.05 ± 0.14	0.03 ± 0.14	0.04 ± 0.17
Semi-arid savanna	CLIM	0.00 ± 0.00	0.00 ± 0.00	0.00 ± 0.00	0.01 ± 0.00
	CO_2	0.00 ± 0.00	0.00 ± 0.00	0.00 ± 0.00	0.00 ± 0.00
	LULCC	0.00 ± 0.00	0.00 ± 0.00	0.00 ± 0.00	0.00 ± 0.00
	NET	0.00 ± 0.00	0.00 ± 0.00	0.00 ± 0.00	0.00 ± 0.00
Desert/Shrubland	CLIM	0.10 ± 0.08	0.03 ± 0.04	0.04 ± 0.02	0.03 ± 0.06
	CO_2	-0.07 ± 0.03	-0.04 ± 0.03	-0.10 ± 0.03	-0.07 ± 0.04
	LULCC	0.02 ± 0.02	0.02 ± 0.03	0.03 ± 0.02	0.05 ± 0.04
	NET	0.04 ± 0.06	0.01 ± 0.03	-0.02 ± 0.05	-0.04 ± 0.05

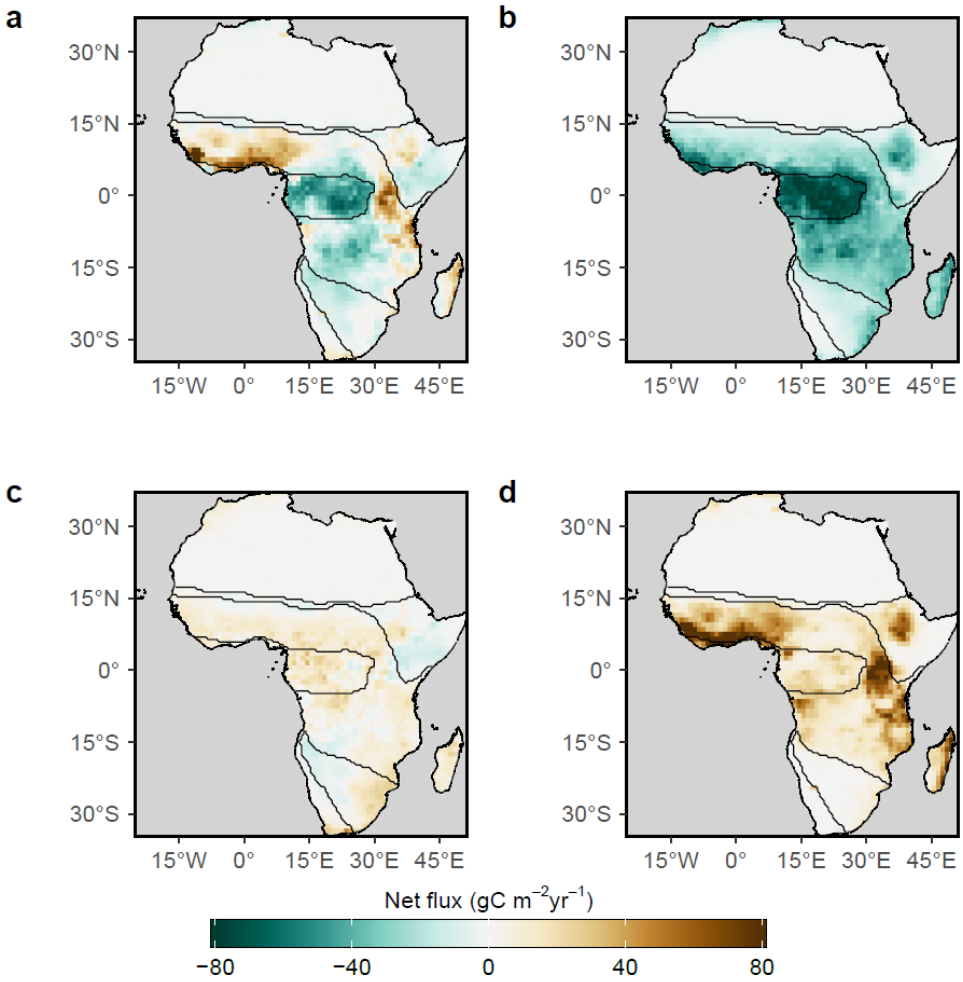

Figure 5. Spatial pattern of trends in annual mean NBP (gC $m^{-2}yr^{-1}$) across Africa over 2000 to 2019 based on an ensemble of 14 DGVMs from TRENDY v9. Large opposing fluxes result in a net sink of carbon (a), while (b) shows the attribution of CO_2 fertilisation and N deposits, (c) the attribution of climate change and variability and (d) the attribution of LULCC. Black isolines represent the boundaries of the ecoregions as depicted in Figure 1.

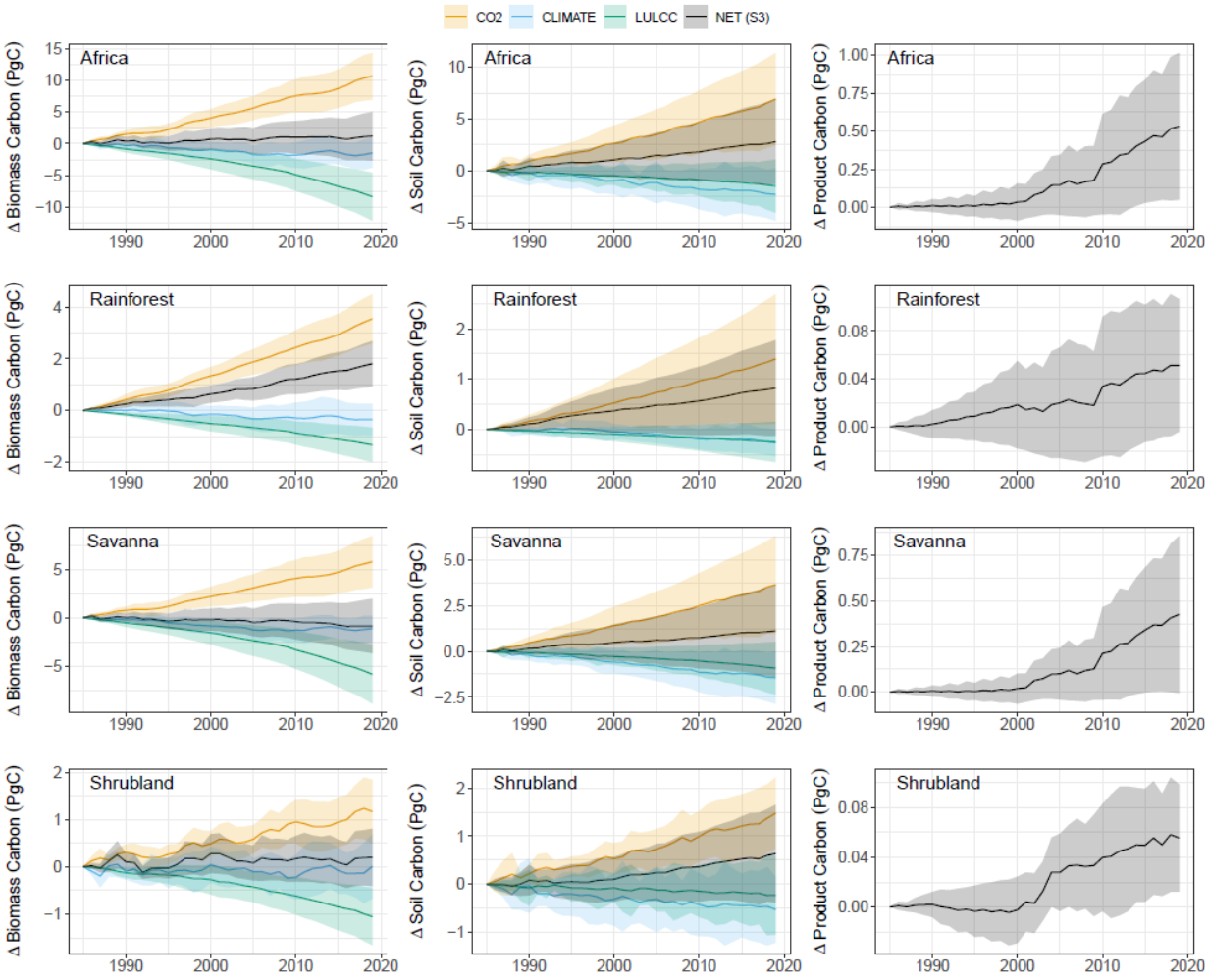

Figure 6. Change in carbon pools over the 1985 to 2019 period.

2.3.3. Ecosystem models without land use (aDVGM)

The aDGVM is an individual-based model that has been developed specifically to simulate grass-tree dynamics in African ecosystems (Scheiter & Higgins, 2009). It has been shown to simulate the distribution of grasslands, savannas, and forests in Africa but detailed assessments of carbon fluxes have not been conducted (Martens et al., 2021; Scheiter & Higgins, 2009). The aDGVM only represents potential natural vegetation without any land use driver (see section 2.3.2 for results including land use). Here aDGVM was forced with an ensemble of regionally-downscaled general circulation models over the 1985-2018 period.

In aDGVM simulated GPP, NPP and NEE increased to 13.4, 7.4, and -3.0 $PgCyr^{-1}$ for the 2009-2018 period (Table 7). These GPP values are lower than estimates from satellite observation (22.4 to 24.7 $PgCyr^{-1}$ for different periods, section 2.3.1, Table 5), and lower than values simulated by other DGVMs (GPP between 20.6 and 40.9 $PgCyr^{-1}$, NPP between 9.2 and 20.5 $PgCyr^{-1}$ for an ensemble of nine models, (Valentini et al., 2014); NPP of 10.2 $PgCyr^{-1}$ for the period 1980-2009 in simulations for Africa, (Pan et al., 2015); NPP of 10.2 and 10.9 $PgCyr^{-1}$ in the presence and absence of fire (Sato & Ise, 2012). However the NEE of the forest region simulated by aDGVM (-0.51 $PgCyr^{-1}$ for 1985-2008, increasing to -0.56 $PgCyr^{-1}$ for 2009-2018) is slightly higher than the estimate of -0.34 PgC yr^{-1} (CI, -0.15 to -0.43) for observation data from sparse forest plots (Lewis et al., 2009). This supports results by Hubau et al., (2020) indicating that the forest carbon sink in intact African forests remained constant throughout the RECCAP2 period.

Both autotrophic and heterotrophic respiration increased for Africa according to aDGVM simulations (Table S3). Autotrophic respiration increased from 1.03 $PgCyr^{-1}$ in the period 1985-2008 to 1.19 $PgCyr^{-1}$ in the period 2009-2018, heterotrophic respiration increased from 8.11 $PgCyr^{-1}$ to 8.82 $PgCyr^{-1}$ over the same periods. Highest respiration rates were simulated in the Sub-humid savanna region (0.65 $PgCyr^{-1}$ and 4.72 $PgCyr^{-1}$ for autotrophic and heterotrophic respiration in 2009-2018). Valentini et al., (2014) report a multi-model mean heterotrophic respiration 11.8 $PgCyr^{-1}$, which is higher than the aDGVM simulations.

In aDGVM simulations, carbon stored aboveground in Africa was 59.5 PgC in the period 2009-2018 (Table 7). This is lower than values by other models; 66.7 to 181.44 PgC for an ensemble of nine models (Valentini et al., 2014); 75.3 to 87.5 PgC with SEIB-DGVM (Sato & Ise, 2012); but falls within the range of estimates (48.3-64.5 PgC) by remote sensing AGB products (Avitabile et al., 2016; Baccini et al., 2012.; Liu et al., 2015; Saatchi et al., 2011). Those remote sensing products do however represent slightly different periods within the RECCAP2 time period.

Aboveground carbon increased by 4.6 PgC between 2009 and 2018 with the highest increases in Sub-humid savannas. Belowground biomass increased by 2 PgC, and SOC increased by 3.1 PgC (Table 7), the overall rate of increase estimated without land use activities is 0.674 $PgCyr^{-1}$ which is higher than for the 1985-2008 period.

Table 7: Carbon stocks and fluxes simulated by aDGVM.

Carbon stocks		**AboveGround (PgC)**		**Belowground (PgC)**		**Soil (PgC)**		**Total (PgC)**		**Trend (PgCyr^{-1})**	
	Region	1985-2008	2009-2018	1985-2008	2009-2018	1985-2008	2009-2018	1985-2008	2009-2018	1985-2008	2009-2018
Total carbon	NH Desert	0.95	1.05	0.59	0.67	4.22	4.33	5.76	6.06	0.016	0.04
	Forest	18.85	19.66	3.68	3.92	12.75	13.29	35.29	36.86	0.083	0.1
	Desert/Shrubland	0.26	0.29	0.13	0.15	1	1.03	1.39	1.47	0.002	0.004
	Sub-humid savanna	28.2	30.97	11.68	12.91	39.32	40.98	79.2	84.87	0.288	0.404
	Semi-arid savanna	6.69	7.58	3.91	4.42	16.37	17.15	26.98	29.14	0.096	0.126
	Africa	54.95	59.54	20.01	22.08	73.66	76.77	148.63	158.4	0.486	0.674
Carbon fluxes								**Total (PgCyr^{-1})**		**Trend (PgCyr^{-1})**	
	Region							1985-2008	2009-2018	1985-2008	2009-2018
NPP	NH Desert							0.23	0.28	0.003	0.012
	Forest							1.15	1.24	0.005	0.006
	Desert/Shrubland							0.06	0.06	0	-0.001
	Sub-humid savanna							3.82	4.14	0.018	0.036
	Semi-arid savanna							1.5	1.68	0.011	0.01
	Africa							6.75	7.4	0.038	0.063
GPP	NH Desert							0.41	0.5	0.005	0.02
	Forest							2.23	2.4	0.01	0.011
	Desert/Shrubland							0.1	0.11	0	-0.002
	Sub-humid savanna							6.86	7.45	0.033	0.066
	Semi-arid savanna							2.63	2.94	0.02	0.018
	Africa							12.22	13.41	0.068	0.114
NEE	NH Desert							-0.06	-0.09	-0.001	-0.008
	Forest							-0.51	-0.56	-0.003	-0.003
	Desert/Shrubland							0	-0.01	0	0.001
	Sub-humid savanna							-1.62	-1.78	-0.01	-0.025
	Semi-arid savanna							-0.52	-0.6	-0.007	-0.005
	Africa							-2.72	-3.04	-0.022	-0.04

Note. Variables are averaged for whole Africa and ecoregions for the periods 1985-2008 and 2009-2018 and stocks include Aboveground, Belowground and Soil. Trends were derived by linear regression models using time series of monthly means of the respective variable. Detailed results in the SI. Some values are zero due to rounding.

2.4. Fluxes of special importance within the African GHG budget

2.4.1. Fires

Recent decades have seen reductions in the area burned per year in Africa from ~3.1 x 10^6 km^2 to ~2.6 x 10^6 km^2 (Andela et al., 2017; Zubkova et al., 2019) and consequently also a decline in total fire emissions (Figure 7) (Van Der Werf et al., 2017). Approximately 30% of this decline is attributed to land transformation and expansion of agricultural land (Zubkova et al., 2019) so does not necessarily imply increased C-sink potential. However the remaining ~70% appears to be a result of higher effective rainfall and soil moisture, particularly in North Africa, producing less flammable vegetation (Zubkova et al., 2019). This decrease in fire, together with CO_2 fertilisation help explain concurrent increases in tree cover (Venter et al., 2018) and increasing GPP trends (section 2.3.3). However, the current burned area products are known to omit small fires and analyses with higher resolution SENTINEL-2 data nearly double the estimated burned area (Roteta et al., 2019), possibly also doubling the estimated GFED fire emissions (Ramo et al., 2021).

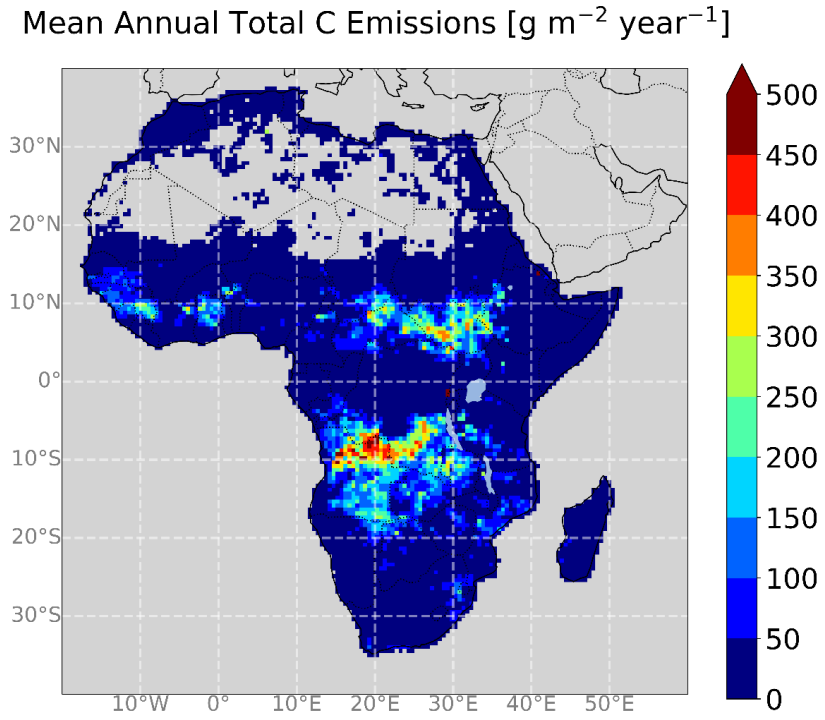

Figure 7. Spatial patterns of biomass burning emissions in Africa, calculated from the FREMV2.1

Existing estimates of total carbon emissions from wildfires for Africa range from 954 to 1595 $TgCyr^{-1,}$ with CH_4 ranging from 4.9 to 9.1 $TgCH_4\ yr^{-1}$ and N_2O from 0.8 to 0.42 $TgN_2O\ yr^{-1}$ (Table 8). Of these emissions, ~85% come from sub-humid savannas which, due to their high productivity and long dry seasons, produce frequent fires that consume high amounts of biomass. Both top-down (calculated via energy released) and bottom-up approaches (calculated via burned area) show a clear decline over the last two decades (Table 8; Figure 8) in the order of ~10 $TgCyr^{-1}$. In contrast, total carbon emissions from wood fuel burning have increased steadily from 184 ± 24.6 $TgCyr^{-1}$ for RECCAP1 to approximately 242 ± 36.1 $TgCyr^{-1}$ for the RECCAP2 period (see Table S4 for more details). This represents an increase of approximately 5.3 $TgCyr^{-1}$. Total fire emissions (wildfire and fuel wood burning) have therefore decreased slightly from 1225 ± 99 to 1197 ± 85 $TgCyr^{-1}$.

A large proportion of these emissions are "carbon-neutral" and offset by rapid regrowth of burned/harvested biomass but when associated with over-harvesting or land conversion some of these emissions represent a net source to the atmosphere (Van Der Werf et al., 2017). Bailis et al., (2015) estimated that ~27% of fuel wood burning in Africa (or approximately 64 TgC) is 'unsustainable', causing a net carbon source. Van Der Werf et al., (2017) estimate that 4% (48 TgC) of the emissions from wildfires in Africa are associated with fires in tropical forests. Burning of crop residue is estimated to add ~22 TgC annually to Africa's carbon emissions (Scholes et al., 2011), so approximately 134 of the 1208 TgC emitted by fires each year could be considered a source.

Table 8: Comparing the change in mean annual emissions ($Tg\ yr^{-1}$) for different chemical species for wildfires (including deforestation and cropland fires) and fuelwood burning over the RECCAP1 and RECCAP2 periods. Fuelwood burning was calculated from published sources (Amos, 1999; Broadhead et al., 2001, Bailis 2005, FAO 2010, Boden 2013) integrated with the IEA World Energy Balances statistics (IEA, 2022).

Type	Source	Region	RECCAP1[a]	RECCAP2 2010-2019	Trend: change/ yr
Wildfire	Valentini	Africa	1031 (+-87)		
	FREMv2.1	Africa	999 (+-79)	953 (+-113)	-10.9
		Northern Hemisphere		377	
		Southern Hemisphere		576	
		Forest		26	
		NH Desert		4	
		SH Desert		3	
		Sub-humid savanna		810	

		Semi-arid savanna		124	
FuelWood	Various[(see SI)]	Africa	184	241	5.3
Total C	**wildfire+fuelwood**		**1215**	**1194**	**-9**
Total CO_2	**FREM (range)**			**3250 (2225-5475)**	
Total CH_4	**FREM (range)**			**6.8 (4.9-9.1)**	
Total C0	**FREM (range)**			**146 (142-224)**	
Total N_2O	**FREM (range)**			**0.09 (0.09/0.42)**	

Note. Estimates come from FREMv2.1, a top-down regional product derived specifically for Africa (slightly modified from Nguyen & Wooster, 2020). Estimates for CO, CH_4 and N_2O emissions for RECCAP2 period are also provided, showing the FREM2.1 estimate and the range of other estimates for that time period. See supplementary information for more details of wildfire emissions data sources and the wood fuel burning estimates.
[a] Valentini et al., (2014) reported from 1997-2011, FREMv2.1 was available from 2004-2009.

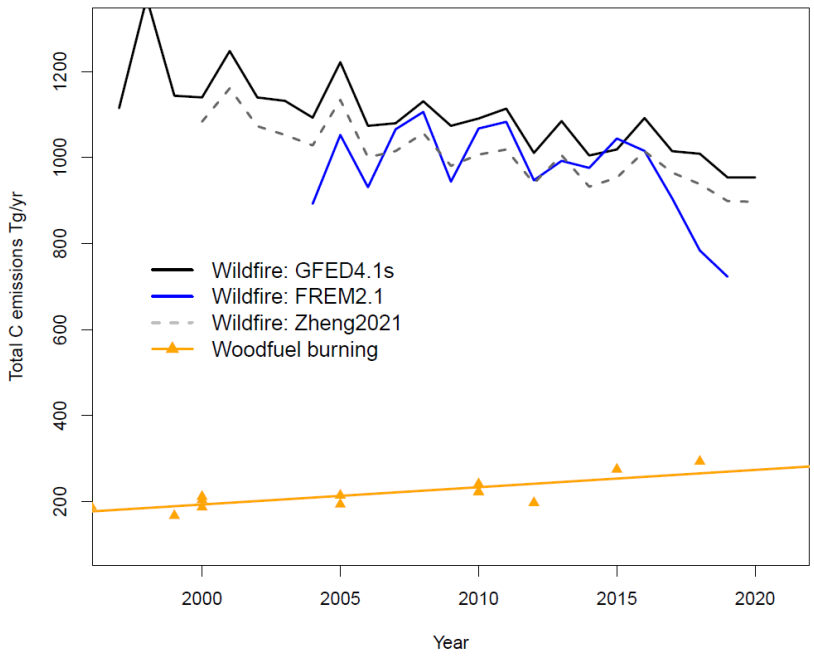

Figure 8. Total carbon emissions from wildfires are decreasing while fuel wood emissions are increasing. Wildfire estimates are provided for a "bottom up" data product (GFED4.1s) (Randerson et al., 2017; Van Der Werf et al., 2017), a global "top-down" data product derived from an atmospheric inversion applied to MOPITT satellite CO data (Zheng et al., 2021), and a regional "top-down" dataset for Africa derived from correlations between FRP and TPM and CO (FREMv2.1 slightly modified from Nguyen & Wooster, (2020)). The trends in these products are consistent but the actual values are still highly uncertain. See Table 8 for the range of current estimates for all greenhouse gases.

2.4.2. Large mammals

Herbivore CH_4 emissions represent a small but increasing component of the African methane cycle (Valentini et al., 2014). Most of these emissions are from livestock, representing 98% of the herbivore biomass in Africa (Hempson et al., 2017), and this is largely enteric fermentation (manure emissions are estimated at < 3% in Africa (Herrero et al., 2008). We therefore only quantified enteric fermentation from livestock. The use of different methodologies and parameterisations, and the lack of accurate information on livestock numbers and production systems add to the uncertainty (Chang et al., 2021; Höglund-Isaksson et al., 2020). Most African countries use the IPCC Tier 1 methodology for reporting livestock emissions (IPCC, 2019). This provides representative emission factors for African livestock production systems, which differ from global averages in terms of diet, average body weights, herd structure, and body condition (Goopy et al., 2021; Ndung'u et al., 2022). The IPCC 2019 methodology estimates emission factors for free-ranging cattle in low productivity systems of Africa to be 48 $kgCH_4$/head yr^{-1} (Table 10.11 in IPCC, 2019), which is much higher than the value of 31 $kgCH_4$/head yr^{-1} previously suggested by IPCC methodologies (Dong et al., 2006). Recent empirical papers from Africa report emissions factors more in line with the original 31 $kgCH_4$/head yr^{-1} (Table 9).

The UNFCCC reporting on livestock emissions is sparse: only 11 of the 52 African countries provided data covering both the 2000-2009 and the 2010-2019 time period. These countries reported methane emissions increasing by ~5% from 5.05 (± 0.32) $TgCH_4yr^{-1}$ to 5.33 (±0.01) $TgCH_4yr^{-1}$ between the two periods. The emissions that were calculated with a standard IPCC 2019 Tier 1 approach were 5.22 and 6.83 $TgCH_4yr^{-1}$ over each time period for the same 15 countries. Hence, UNFCCC estimates and IPCC Tier1 estimates were similar for the 2000-2009 period but the UNFCCC data suggest a 5% increase in emissions while increases using the IPCC Tier 1 approach are closer to 30%. The large increases reported using the IPCC Tier 1 approach are a result of FAO livestock numbers increasing by 30% in the last decade. We produced a new African livestock emission factor (Africa_EF) calculated using the mean of a range of empirical data sources from African livestock production systems (see Table S5) of 35.6 $kgCH_4$/head yr^{-1}. When using Africa_EF instead of the IPCC value of 48 $kgCH_4$/head yr^{-1} the overall methane emissions are reduced, but the increasing trend remains the same.

Herrero et al., (2008) classified 6 different livestock production systems for Africa and used a detailed metabolically-based methane emissions model and modelled livestock numbers from 2000 to 2030. Their estimates are less than half the IPCC 2019 Tier 1 approach (Table 9) and only show a 13% increase between the two periods caused both by increasing livestock numbers and a switch to more mixed production systems. Wolf et al., (2017) modelled global livestock emissions using a Tier 2 approach and revised parameterisations, and estimated emissions for Africa in 2011 to be 12.69 ±

1.94 $TgCH_4yr^{-1}$. Thus, the current best estimate of CH_4 emissions from enteric fermentation of livestock in Africa for the RECCAP2 period is 17.6 (range 9.2- 21.7) $TgCH_4yr^{-1}$ which represents an annual increase of 2.9% (395 $GgCH_4yr^{-1}$) from RECCAP1.

Table 9: Estimates of annual enteric methane emissions ($TgCH_4$ yr^{-1}) for Africa calculated using the IPCC Tier 1 methodology (IPCC2019) and the Tier 1 methodology with Africa-specific emissions factors (IPCC2019_AfricaEF), contrasted with estimates from published sources, and from national UNFCCC reporting.

		2000-2009	2010-2019	Trend: $GgCH_4$ yr^{-1}
UNFCCC (11 reporting countries)				
	UNFCCC	5.1 (+- 0.32)	5.3 (+- 0.1)	27
	IPCC2019	5.2	6.8	161
	IPCC2019_AfricaEF	4.1	5.4	131
Africa				
	Herrero(2008)	8.1	9.2	109
	Wolf (2017)	12.69 ± 1.94		
	IPCC2019	16.8	21.7	482
	IPCC2019_AfricaEF	13.7	17.6	395

Note. IPCC2019 uses emission factors from Table 10.11 which has a cattle emission factor of 48 for low-productivity systems. This is higher than all published emission factors for free-ranging cattle in Africa (See Table S5, so the IPCC2019_AfricaEF replaces this with the mean reported value of 35.6 $kgCH_4$/head yr^{-1}. Only 11 countries have UNFCCC data for both RECCAP periods so data are reported for these 11 countries, and for Africa as a whole.

2.4.3. Termites

Termites are an important source of methane due to the methanogenic degradation of lignocellulose in termite hindguts (Brune, 2014). The African continent hosts 39% of the total 2600 species that have been described worldwide (Ahmed et al., 2011), contributing substantially to global termite CH_4 emissions. Here, we provide new estimates of termite CH_4 emissions across the African continent (Figure 9, Table 10) based on a new global termite biomass product predicted from 500 field transect measurements using a machine learning approach and the global mean and median of termite CH_4 production rate from existing literature (mean = 3.74 μgCH_4g^{-1}[termite] h^{-1}, median = 2.88 μgCH_4g^{-1}[termite] h^{-1}, n = 251) (Zhou et al., 2023). Overall, termites across the African continent are predicted to emit 1.40 $TgCH_4yr^{-1}$ (the 95% confidence intervals range: 1.31-1.49 $TgCH_4yr^{-1}$) based on the mean termite CH_4 production rate, with the largest emission from sub-humid savannas (0.63 $TgCH_4yr^{-1}$) followed by semi-arid savanna (0.37 $TgCH_4yr^{-1}$) and forests (0.19 $TgCH_4yr^{-1}$) (also see Table 10 for the median estimate of termite CH_4 production rate).

This new estimate is substantially lower than the estimate of 2.09 $TgCH_4yr^{-1}$ from the global methane budget (Saunois et al., 2020) (Table 10) and other reported values (2.5 to 6.9 $TgCH_4yr^{-1}$) from Valentini et al., (2014) for the African continent. Two prominent reasons for these inconsistencies are

the lack of accurate data on termite biomass for upscaling, and the scarcity of empirical data on termite CH_4 emission rates. Termite biomass is generally estimated by its dependence on GPP of ecosystems based on simple regression models (Kirschke et al., 2013; Saunois et al., 2020). Here, our global termite biomass estimate is based on available field measurements and predicted by a set of variables, including rainfall, soil pH, NPP, minimum/maximum temperature, soil organic carbon, and topography. Additionally, only a few studies measured CH_4 emission rates at the individual species or mound scale across the African continent (Table S6) with CH_4 emission rates varying significantly between species (0.68-17.4 μg CH_4 g^{-1} h^{-1}), between mounds (81-5478 ng CH_4 s^{-1} $mound^{-1}$) (Brauman et al., 2001; Macdonald et al., 1999; Rouland et al., 1993) and between seasons (Räsänen et al., 2023). However, more empirical measurements are still needed to improve the accuracy of termite biomass as well as termite methane emission rates across different ecosystems and regions.

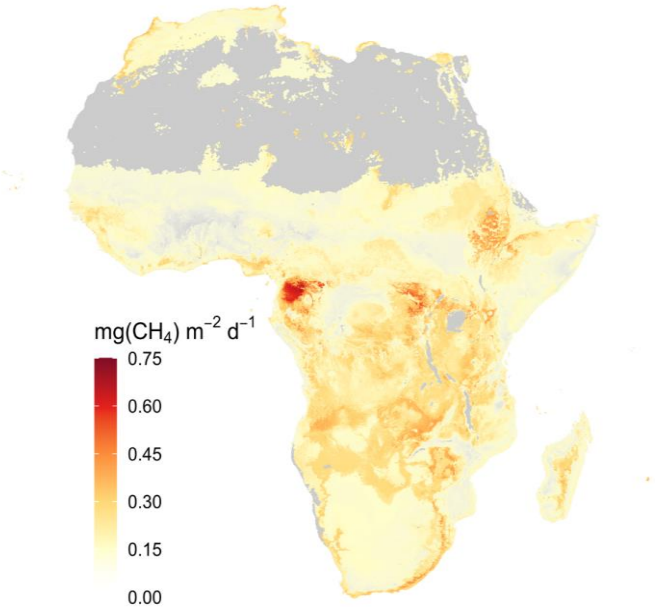

Figure 9. Methane emission rates ($mgCH_4$ m^{-2} d^{-1}) from termites estimated across the African continent.

Table 10. Predicted termite methane emissions across African ecoregions. Values in parentheses represent the 95% confidence intervals.

Ecoregion	**Termite methane emissions ($TgCH_4$ yr^{-1})**		
	Saunois et al. (2020)	New estimate based on mean termite CH_4 production rate	New estimate based on median termite CH_4 production rate
North Africa desert	0.067	0.134 (0.123-0.145)	0.103(0.094-0.111)
Desert/shrubland	0.021	0.039 (0.036-0.042)	0.030(0.028-0.032)
Semi-arid savanna	0.354	0.367 (0.342-0.392)	0.282(0.263-0.301)
Sub-humid savanna	1.220	0.629 (0.589-0.670)	0.484(0.452-0.516)
Forest	0.350	0.185 (0.175-0.195)	0.142(0.134-0.150)
Africa (in total)	**2.094**	**1.397 (1.305-1.489)**	**1.076(1.004-1.247)**

2.5. Component fluxes of NEE from geological, aquatic, and coastal systems

2.5.1. Geological carbon emissions

Africa's geogenic CO_2 emissions are mostly due to volcanic and geothermal activity in the East African Rift (EAR) which is globally the largest active continental rift, spanning a cumulative length of approximately 3000 km (Lee et al., 2016). Extrapolation from first-order CO_2 flux measurements of tectonic degassing in the Magadi-Natron basin, amounts to a flux of 71 ± 33 $TgCO_2\ yr^{-1}$ in the EAR (Lee et al., 2016). However, estimates based on extrapolation from surveys in the Main Ethiopian Rift (0.52–4.36 $TgCO_2yr^{-1}$) gives a flux range of 3.9–32.7 $TgCO_2yr^{-1}$ (Hunt et al., 2017).

Geological emission sources of CH_4 were calculated for each ecoregion and Africa as a whole using data from Etiope et al. (2019) (Table 11, Table S7). These include emissions from onshore seeps (gas-oil seeps and mud volcanoes), diffuse exhalation of CH_4 associated with petroleum fields (microseepage) and geothermal manifestations mainly from volcanoes and geothermal sites, but excluding submarine seeps (see Ciais et al., 2022). The North African desert ecoregion contributes 46% of the estimated total African geological CH_4 emissions of 1.01 $TgCH_4yr^{-1}$ (see Figure S1 for the spatial distribution). Semi-arid and Sub-humid savanna ecoregions contribute 30% and 20% respectively while the forest ecoregion only contributes 5% of the estimated geological CH_4 emissions across Africa.

2.5.2. Weathering uptake of atmospheric CO_2

We extracted estimates of weathering CO_2 uptake and the weathering dissolved inorganic carbon (DIC) release from gridded products provided by Lacroix et al., (2020) for the African ecoregions (Table 11, Table S8). The method quantifies weathering and depends on surface runoff and temperature, lithology types and soil shielding, and is based on a modified version of the weathering model of Hartmann et al., (2009). Weathering on the continent induces a flux of -12.2 $TgCyr^{-1}$ of CO_2, accounting for around 7 % of the global weathering consumption. The sink estimate for the continent is comparable with the previous estimate of -11.7 $TgCyr^{-1}$ of (Ludwig et al., 1998). The carbon uptake from the atmosphere and carbon originating from the rock material add up to a total of -15.2 $TgCyr^{-1}$ DIC exported to freshwaters and the ocean. Lacroix et al., (2020) reported that there was a general underestimation of catchment DIC exports for African catchments, e.g., a 20% underestimation compared to measurements for the Congo basin.

In Africa, lowest consumption rates (0 – 0.1 $tC\ km^{-2}\ yr^{-1}$) were recorded over eastern and southern Africa, while larger amounts (0.5 – 5 $tC\ km^{-2}\ yr^{-1}$) of CO_2 were consumed in central Africa and parts of East Africa. The Semi-arid savanna ecoregion, which consists, to a large degree, of metamorphics,

unconsolidated and silicoclastic sediment lithological classes, accounts for the highest weathering rates per area and the largest part of the continent's weathering drawdown and DIC release (Table 11, Table S8), owing to rather high runoff rates ranging from 50 to 250 mm yr^{-1}. Weathering rates in warm and runoff-abundant tropical forest areas are strongly reduced due to shielding by old and highly weathered soils (Hartmann et al., 2014), whereas weathering in the dry semi-arid savanna and desert is limited by precipitation and runoff, which is dominantly less than 25 mm yr^{-1}.

2.5.3. Inland water emissions

The inland water network serves as a major conduit for transfers of C and N, which were originally fixed by terrestrial ecosystems from the atmosphere, to the ocean. Inland waters are at the same time biogeochemical reactors for the terrestrial C and N loads, driving an important production and emission of GHGs. Finally, a part of the terrestrial C inputs to rivers are buried in aquatic sediments. The emissions of C from inland waters to the atmosphere (in the forms of CO_2 and CH_4) represent a return loop in the land-atmosphere C balance which is not necessarily included when upscaling from for instance flux tower observations. Moreover, the increased production and emission of the more potent GHG CH_4 under anaerobic conditions in aquatic sediments gives inland waters an important role in the GHG budget of continents. Fluvial exports of C to the coast and burial of C in aquatic sediments, on the contrary, add to the net uptake of atmospheric C on the continents.

Emissions of CO_2, CH_4 and N_2O from rivers and lakes were taken from the regional estimates by Borges et al. (2015, 2022) which provide average annual emissions of 990-1360 $TgCO_2yr^{-1}$, 3.9-5.2 $TgCH_4yr^{-1}$ and 14.8-19.8 GgN_2Oyr^{-1} from African rivers, and annual emissions of 12.1 $TgCO_2yr^{-1}$ and 2.2 $TgCH_4yr^{-1}$ from African lakes, but explicitly excluded reservoirs (Table 11). Moreover, they suggest that African lakes can be a minor sink of 0.2 GgN_2Oyr^{-1} (Borges et al., 2022). For reservoir emissions, we used numbers provided in the synthesis of regionalised inland water emissions estimates by Lauerwald et al. (2023) for the RECCAP2 initiative. These estimated emissions amount to 16 (7/26) $TgCO_2yr^{-1}$, 2.1 (1.2/3.1) $TgCH_4yr^{-1}$ and 6.6 (2.7/8.6) GgN_2Oyr^{-1} (Lauerwald et al., 2023). Summing up these estimates, we get to total emission fluxes of 1,203 $TgCO_2yr^{-1}$, 8.9 $TgCH_4yr^{-1}$ and 23.7 GgN_2Oyr^{-1} from African inland waters (Table 11). It is noteworthy that rivers contribute 98% of inland water CO_2 emissions, but only about half of inland water CH_4 emissions.

To quantify DOC and POC we summarised data from Zscheischler et al., (2017), and freshwater burial was quantified from Mendonça et al., (2017).

2.5.4. Fluxes from estuaries and coastal wetlands

Emissions of CO_2, CH_4, and N_2O from various coastal ecosystems in Africa were estimated using available empirical data scaled to the total surface area of each of the coastal ecosystems (Table 11).

These systems include tidal systems and deltas, lagoons, mangroves, salt marshes and seagrasses. Organic carbon burial and coastal margin (non-riverine) C inputs were also estimated. However, although the coastal margin C sink is likely to be substantial, methodology are not yet resolved enough to calculate at the regional scale. To deal with this highly uncertain estimate we therefore included the (rough) estimate in Table 11 for reporting purposes but for the final budgets we set the mean value to zero and the 95th quantile as our best estimate. Hereby, the coastal margin sink is not represented in the final budgets but the uncertainty has been accounted for.

Table 11. Geological, Inland Water and Coastal CO_2, CH_4, N_2O and net GHG emissions and sinks.

	CO_2 (Tg yr^{-1})	**CH_4 (Tg yr^{-1})**	**N_2O (Gg yr^{-1})**	**CO_2eq (GWP100) (Tg yr^{-1})**	**C (Tg yr^{-1})**
Geological sources [a]	**18.3 (3.9/32.7)**	**1 (1/1)**		**45.7 (31.3/60.1)**	**5.8 (1.8/9.7)**
Atmospheric fluxes					
Lakes [b]	12.1 (12.1/12.1)	2.2 (2.2/2.2)	-0.2 (-0.2/-0.2)	71.4 (71.4/71.4)	5 (5/5)
Reservoirs [c]	16.2 (6.8/26.1)	2.1 (1.2/3.1)	6.6 (2.7/8.6)	74.7 (39.9/111)	5.7 (1.9/9.4)
Rivers [b]	1175 (990/1360)	4.6 (3.9/5.2)	17.3 (14.8/19.8)	1302.6 (1099.3/1505.8)	322.4 (271.7/373.1)
Estuary Emissions (Tidal systems and lagoons) [d]	21.6 (12.7/32.4)	0 (0/0.1)	2.8 (2.5/3.2)	23.3 (13.4/37.3)	5.9 (2.5/9.6)
Coastal Wetland Emissions (Mangroves, Salt marshes, Seagrasses) [d]	-118.8 (-149.1/-82)	0.1 (0.1/0.3)	0.1 (0.1/0.3)	-116 (-147.1/-73.4)	-32.4 (-45.8/-22.5)
Net aquatic atmospheric fluxes	**1106.2 (872.5/1348.6)**	**9 (7.4/10.9)**	**26.6 (19.8/31.8)**	**1356.1 (1076.9/1652.2)**	**306.6 (235.2/374.7)**
Carbon stock change					
OC burial – inland [e]	-131.9 (-24.1/-212.6)	0 (0/0)	0 (0/0)	-131.9 (-24.1/-212.6)	-36 (-6.6/-58)
OC burial - coastal [d]	-20.9 (-20.9/-20.9)	0 (0/0)	0 (0/0)	-20.9 (-20.9/-20.9)	-5.7 (-5.7/-5.7)
Net aquatic carbon stock change	**-152.8 (-45/-233.5)**	**0 (0/0)**	**0 (0/0)**	**-152.8 (-45/-233.5)**	**-41.7 (-12.3/-63.7)**
Lateral fluxes					
DIC [f]	-55.7 (-55.7/-55.7)	0 (0/0)	0 (0/0)	-55.7 (-55.7/-55.7)	-15.2 (-15.2/-15.2)
DOC [g]	-71.4 (-71.4/-71.4)	0 (0/0)	0 (0/0)	-71.4 (-71.4/-71.4)	-19.5 (-19.5/-19.5)
POC [g]	-64.6 (-64.6/-64.6)	0 (0/0)	0 (0/0)	-64.6 (-64.6/-64.6)	-17.6 (-17.6/-17.6)
Coastal Margin C inputs [d]	-458.3 (-187/-729.7)	0 (0/0)	0 (0/0)	-458.3 (-187/-729.7)	-125 (-51/-199)

Net aquatic lateral fluxes	**-650 (-378.6/-921.3)**	**0 (0/0)**	**0 (0/0)**	**-650 (-378.6/-921.3)**	**-177.3 (-103.3/-251.3)**

[a] Hunt et al. 2017, Etiope et al. 2017, section 2.5.1
[b] Borges et al. 2015, 2022
[c] Lauerwald et al. 2023
[d] RECCAP2 database (https://www.bgc-jena.mpg.de/geodb/projects/Data.php)
[e] Mendonça et al 2017
[f] Lacroix et al., 2020, section 2.5.2
[g] Zscheischler et al. 2017

2.6. Trade fluxes

2.6.1. Carbon in crop and wood trade

The transfer of physical and embodied carbon to and from Africa represents a relatively small percentage when compared to the rest of the world (Peters et al., 2012). We consider the physical flows of carbon via trade in biomass that includes crops and harvested wood products for three different periods, including 1961-1984, 1985-2008 and 2009-2019, based on inventory data from the Food and Agricultural Organisation of the United Nations (FAO; https://www.fao.org/faostat/en/#data, accessed 18 October 2023). F_{trade} is considered a carbon flux source by the region if it imports more than it exports or a carbon flux sink if otherwise.

Africa was a net importer of crops during all three periods (Table 12). Carbon imports through crops have increased more than six-fold in the 1985 to 2008 period from the 1961 to 1984 period and almost doubled from the 1985-2009 to 2010-2019 periods. From 1961 to 2009, Africa was a small net exporter of carbon through wood. During the RECCAP2 period, however, Africa's wood carbon imports exceeded the exports, although the amount of carbon entering the region was still relatively small in contrast to global carbon trade.

Table 12. Crop and wood trade fluxes (± inter-annual variability) in $TgCO_2yr^{-1}$ and $TgCyr^{-1}$. Positive values represent imports (source) and negative values represent exports (sink).

Period	**1961-1984**		**1985-2009**		**2010-2019**	
	$TgCO_2yr^{-1}$	$TgCyr^{-1}$	$TgCO_2yr^{-1}$	$TgCyr^{-1}$	$TgCO_2yr^{-1}$	$TgCyr^{-1}$
Crop export	-13.63 ± 2.34	-3.68 ± 0.63	-14.93 ± 4.02	-4.03 ± 1.09	-29.13 ± 10.84	-7.87 ± 2.93
Crop import	22.60 ± 13.16	6.10 ± 3.55	73.55 ± 23.88	19.86 ± 6.45	137.22 ± 45.33	37.22 ± 12.24
Crop Net flux	**8.97 ± 13.37**	**2.42 ± 3.61**	**58.62 ± 24.22**	**15.83 ± 6.54**	**108.74 ± 46.61**	**33.2 ± 12.59**
Wood export	-3.88 ± 0.72	-1.05 ± 0.19	-7.66 ± 3.28	-2.07 ± 0.89	-9.89 ± 3.27	-2.70 ± 0.88
Wood import	1.64 ± 0.63	0.44 ± 0.17	4.22 ± 2.26	1.14 ± 0.61	9.93 ± 3.59	2.68 ± 1.00
Wood Net flux	**-2.25 ± 0.96**	**-0.6 ± 0.26**	**-3.44 ± 3.98**	**-0.9 ± 1.07**	**0.048 ± 4.86**	**0.3 ± 1.33**

2.7. Anthropogenic emissions of greenhouse gases from inventory data

In RECCAP1, Valentini et al. (2014) used the UNFCCC data to derive estimates for anthropogenic emissions. However, due to the sparse reporting of countries in Africa, we summarise the GHG emission estimates provided by the International Energy Agency acquired through Climate Watch (https://www.climatewatchdata.org/, accessed 18 October 2023). Total fossil fuel emissions increased from 1.216 $PgCO_2$-eq to 1.728 $PgCO_2$-eq from the 1990-2009 to 2010-2019 period (Table 13). Fossil fuel emissions contributed 42% of the total anthropogenic emissions while LULCC contributed about 32% during RECCAP2. We therefore notice that the proportional contribution of fossil fuel emissions has increased since RECCAP1 (39% and 35% contribution for fossil fuels and LUCF, respectively). Of the 23% contribution of agriculture (including livestock) to the total emissions, methane emissions are responsible for 15%. For a comprehensive analysis and comparison of inventory data to atmospheric inversions for Africa, see Mostefaoui et al., (2023).

Table 13. Anthropogenic greenhouse gas emissions for the 1990-2009 (R1) and 2010-2019 (R2) periods.

		Anthropogenic emissions ($PgCO_2$-equivalent yr^{-1})					
	Period	**Fossil fuels (including industrial processes)**	**Waste**	**Agriculture**	**LUCF**	**Total incl LUCF**	**Bunkers (Tg CO_2-eq yr^{-1})**
CO_2	R1	0.83 ± 0.11			0.98 ± 0.02	1.81 ± 0.13	37.1 ± 3.83
	R2	1.28 ± 0.06			1.20 ± 0.07	2.48 ± 0.12	41.6 ± 1.69
CH_4	R1	0.35 ± 0.04	0.13 ± 0.02	0.44 ± 0.05	0.06 ± 0.02	0.99 ± 0.08	0.04 ± 0.01
	R2	0.38 ± 0.02	0.16 ± 0.01	0.61 ± 0.03	0.06 ± 0.00	1.21 ± 0.04	0.02 ± 0.01
N_2O	R1	0.06 ± 0.02	0.01 ± 0.00	0.28 ± 0.03	0.04 ± 0.01	0.36 ± 0.05	0.24 ± 0.03
	R2	0.08 ± 0.00	0.02 ± 0.00	0.36 ± 0.01	0.05 ± 0.00	0.46 ± 0.01	0.28 ± 0.02
Total	**R1**	**1.23 ± 0.12**	**0.15 ± 0.02**	**0.73 ± 0.06**	**1.09 ± 0.03**	**3.15 ± 0.16**	**37.4 ± 3.83**
	R2	**1.74 ± 0.06**	**0.19 ± 0.01**	**0.97 ± 0.03**	**1.31 ± 0.07**	**4.15 ± 0.12**	**41.9 ± 1.69**

2.7.1. Emissions from different fossil fuel energy sources

We used the Greenhouse Gas from Energy Database Highlights data set (IEA, 2023) to evaluate the greenhouse gas emissions from different energy sources (Figure 10). The data in Table 14 show that fuel combustion from coal, gas and oil increased substantially from 1985-2009 to 2010-2019 while the increasing trend for fugitive emissions seems to slow down for the RECCAP2 period, but still contributing almost the same amount of emissions as for RECCAP1. Emissions from bunkers add a relatively small amount of emissions to the total estimate, with emissions increasing for aviation bunkers and decreasing for marine bunkers from 1985-2008 to 2009-2019.

Table 14. Emission estimates ($TgCO_2$-eq yr^{-1}) for different fossil fuel energy sources.

Energy source	1985-2009	2010-2019
Coal - Fuel combustion	276.51 ± 59.43	399.06 ± 18.29
Oil - Fuel combustion	298.85 ± 62.37	522.65 ± 38.78
Gas - Fuel combustion	95.03 ± 44.38	233.78 ± 30.50
Fugitive emissions	337.91 ± 57.02	340.63 ± 20.10
Marine bunkers (CO_2 only)	19.65 ± 3.91	18.55 ± 0.97
Aviation bunkers (CO_2 only)	15.34 ± 3.50	23.85 ± 1.01

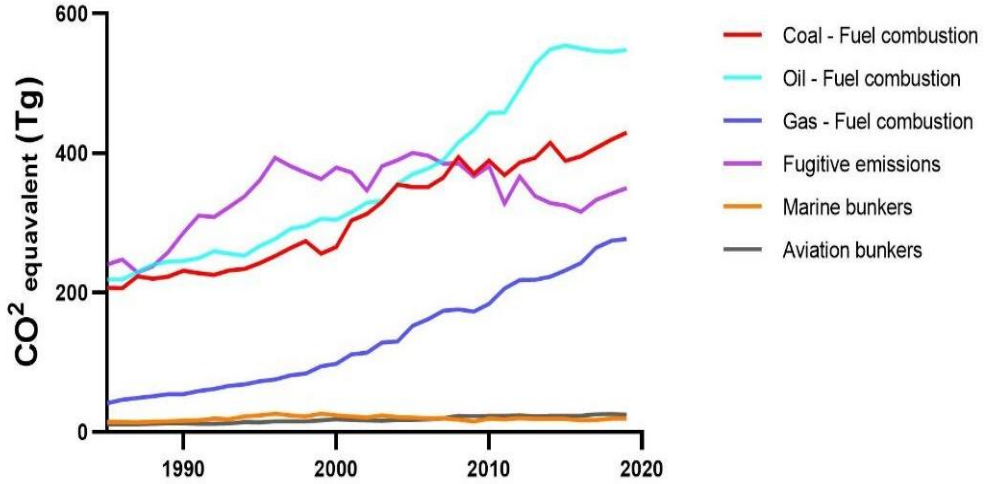

Figure 10. Fossil fuel (and biofuel) emissions by fuel type.

2.8. Results of top-down atmospheric inversions

2.8.1. CO_2 inversions

For the land CO_2 fluxes, we used a set of four CO_2 inversions that used data from the global surface in situ network: CAMS v20r2 (Chevallier et al., 2005, 2019), sEXTocNEET_v2021 (Rödenbeck et al., 2003, 2018), Carbon Tracker Europe CTE2021 (Van Der Laan-Luijkx et al., 2017), University of Edinburgh or UoE (Feng et al., 2016) and one inversion driven by both in-situ and satellite column-averaged dry air mole fraction of atmospheric CO_2 from OCO-2 and GOSAT: CMS-Flux (Liu et al., 2021), all with different priors, algorithms and transport and re-analyses fields, described in the global carbon budget 2021 (Friedlingstein et al., 2022) (Figure 11). Previous synthesis studies showed that the net terrestrial carbon balance of Africa is a small CO_2 sink (Ciais et al., 2011; Valentini et al., 2014; Williams et al., 2007). However, the inversions are subject to large uncertainties, especially in the tropics, because of the lack of observations and the difficulties of representing tropical convection and related vertical mixing (Gaubert et al., 2019; Schuh et al., 2019). Using satellite CO_2 column retrievals, (Palmer et al., 2019) identified northern tropical Africa as being responsible for the

majority of the pan-tropical net carbon seasonal cycle, with the largest emissions found over western Ethiopia and western tropical Africa during March and April.

In RECCAP1, the spread of the net exchange carbon according to four inversions was 1 PgC yr^{-1} for five years' annual means (2001-2004). Based on our collected CO_2 inversions, the standard deviation was 0.25 PgC yr^{-1} for both 2001-2004 and for 2000-2009, and 0.30 PgC yr^{-1} for 2010-2019 (Table 15). For the 2000-2009 period, the average land flux (sink) was -0.14 PgC yr^{-1} ± 0.25 PgC yr^{-1} with three out of four inversions showing moderate CO_2 uptake through the entire decade. In contrast, the same four inversion models find the 2010-2019 period to be a carbon source (0.11 ± 0.27 PgC yr^{-1}) to the atmosphere, likely as a result of the 2015/2016 El-Niño with most inversions showing a net source in 2016 with an average flux of 1 PgC yr^{-1}(Table 15). This source is in line with previous studies that identify increased respiration rates associated with the increased surface-temperature in 2016 (Gloor et al., 2018; Liu et al., 2017). For the full set of five available inversion models used for the 2009-2019 period, this source is estimated at 0.27 ± 0.3 PgC yr^{-1} as the CMS-flux inversion model estimates net emissions over most of this period. Within Africa, this source is mostly driven by emissions from the sub-humid savanna (0.27 ± 0.19 PgC yr^{-1}). The CMS-Flux inversion is driven by GOSAT and OCO-2 data and show a larger source than the in-situ inversions alone. This source is driven by satellite observations of high CO_2 over northern tropical Africa during the dry season and might be overestimated (Gaubert et al., 2023).

Table 15. Inverse model ensemble summary of posterior land fluxes for CO_2 **(**PgC yr^{-1}). A positive value means a source to the atmosphere.

	2010-2009 (4 inversions)			**2010-2019 (4 inversions)**			**2010-2019 (5 inversions)**		
	mean	stdev	range	mean	stdev	range	mean	stdev	range
African continent	-0.14	0.25	-0.35/0.37	0.11	0.27	-0.07/0.29	0.27	0.3	-0.07/0.93
Desert/Shrubland	0	0	-0.01/0.	0	0	-0.01/0.01	0	0	-0.01/0.01
Forest	-0.05	0.05	-0.13/0.07	-0.03	0.07	-0.16/0.06	-0.05	0.06	-0.16/0.06
North-Africa desert	0	0.01	-0.04/0.02	-0.01	0.01	-0.04/0.01	-0.01	0.01	-0.04/0.01
Semi-arid savanna	-0.03	0.05	-0.07/0.01	0.05	0.06	-0.01/0.15	0.07	0.06	-0.01/0.15
Sub-humid savanna	-0.06	0.16	-0.23/0.29	0.09	0.15	-0.1/0.25	0.27	0.19	-0.1/0.98

Note. Value for 2009-2019 for all 5 available inversions are also shown (column 3), but for assessing change since the previous decade it is more appropriate to compare data with only 4 inversions.

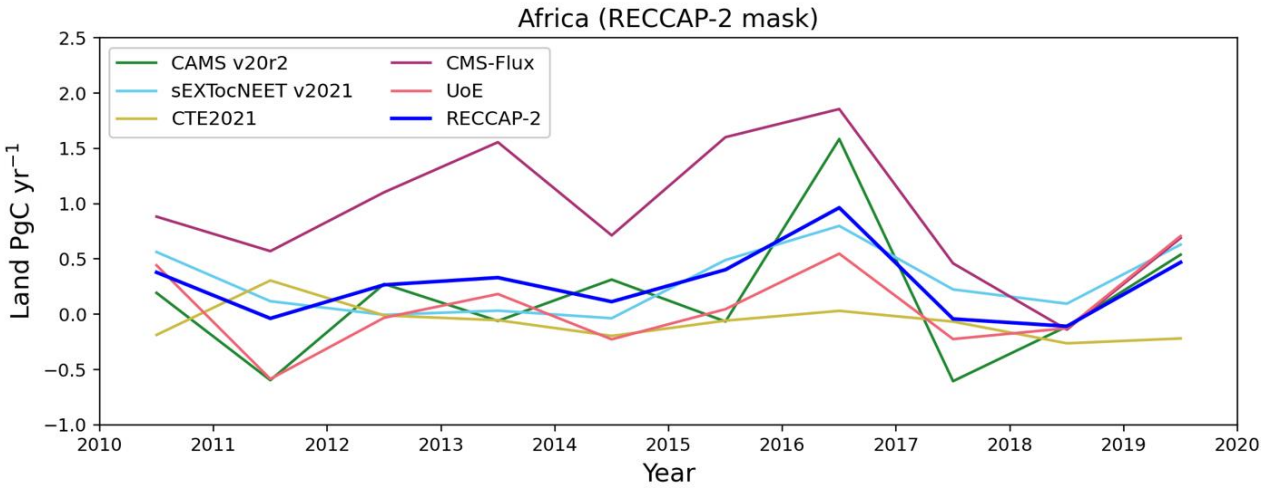

Figure 11. Annual land CO_2 fluxes (represented as year + 0.5) over Africa **(**PgC yr^{-1})

2.8.2. CH_4 and N_2O inversions

We present an inter-comparison of six surface-based atmospheric inversion models for CH_4 over Africa and four inversions with assimilation of GOSAT observations with different transport models and inversion techniques CT-CH_4/SURF (Tsuruta et al., 2017), NICAM-TM/4DVar (Niwa et al., 2017), NIES-TM-FLEXPART (Maksyutov et al., 2021; Wang et al., 2019), TM5-CAMS (Bergamaschi et al., 2010, 2013; Pandey et al., 2016; Segers & Houwelling, 2018), TM5-4DVAR (Bergamaschi et al., 2013; Bergamaschi et al., 2018). The comparison reveals a significant model estimate range difference of over 15 $TgCH_4yr^{-1}$ in annual mean estimates for Southern Africa (Table 16). The inversion results from surface based ensemble mean estimates for North Africa between 2009 and 2017 was 25.94 ± 3.03 $TgCH_4yr^{-1}$, and for Southern Africa, it was 52.08 ± 5.05 $TgCH_4yr^{-1}$ (Table 16). These values are slightly larger than the mean methane emissions during the previous period 2000-2008, which were 23.02 ± 3.76 $TgCH_4yr^{-1}$ for North Africa, and 49.37 ± 3.81 $TgCH_4yr^{-1}$ for Southern Africa. This is nearly 5% for North Africa and 12% for Southern Africa of the global total methane estimate of 557 $TgCH_4yr^{-1}$ (Wang et al., 2019).

GOSAT based inversions show similar estimates to the surface based inversions. Mean estimates of four GOSAT-based inversions were 23.14 ± 2.29 $TgCH_4yr^{-1}$ for Northern Africa, and 57.66 ± 5.68 $TgCH_4yr^{-1}$ for Southern Africa for the years 2010-2017 (Table 16). Although Africa's contribution to global methane emissions is relatively small, it is important to monitor the continent's emissions as they may increase in the future due to population growth, urbanization, and the development of oil and gas production. Agricultural west and wetlands are responsible for more than 80% of net methane emissions in Africa.

The spatial mean estimations of N_2O concentrations in Africa, as reported by five inversion models, have shown a relatively small discrepancy with a mean value of 3.26 ± 0.19 $TgNyr^{-1}$ during the years from 2000 to 2008 (Table 16). This value has slightly increased to 3.44 ± 0.14 $TgNyr^{-1}$ from 2009 to 2016. The data from these models showed similar results over these two time periods, with a small increase in the average N_2O concentrations.

Table 16. Inversion estimates include the model means, variance and ranges for CH_4 and N_2O.

CH_4	**2000-2008**			**2009-2017**		
(6 Surface-based inversions)	Mean	Model variance	Range	Mean	Model variance	Range
Africa	72.39	2.91	68.56 - 75.53	78.02	3.88	73.04 - 82.90
North Africa	23.02	3.76.	19.01 - 27.84	25.94	3.03	22.86 - 30.25
Southern Africa	49.37	3.81	45.56 - 54.99	52.08	5.05	45.73 - 60.03
CH_4	**2000-2008**			**2009-2017**		
(GOSAT inversions)	Mean	Model variance	Range	Mean	Model variance	Range
Africa	–	–	–	80.80	6.45	73.16 - 87.11
North Africa	–	–	–	23.14	2.29	21.20 - 26.34
Southern Africa	–	–	–	57.66	5.68	51.31 - 63.85
N_20	**2000-2008**			**2009-2016**		
	Mean	Model variance	Range	Mean	Model variance	Range
TgN	3.26	0.19	3.40 - 3.53	3.44	0.14	3.29 - 3.61
TgN_2O	5.1182	0.2983	5.338 – 5.5421	5.4008	0.2198	5.1653 – 5.6677

3. Synthesis of the African region greenhouse gases budget

We summarised the estimates and trends for the African GHG flux components and carbon stocks for the RECCAP2 period (Table 17). We present separate total estimates for each of the gases (CO_2, CH_4, N_2O) and calculated the Carbon ($PgCyr^{-1}$) and GHG budgets in CO_2 equivalents using the GWP100 values from the IPCC sixth assessment (IPCC, 2021). We employed both bottom-up (BU) and top-down (TD) approaches as described by Ciais et al., (2022) and compare these estimates below. Uncertainty estimates, calculated as the 5^{th} and 95^{th} percentiles, are provided in brackets where possible. Uncertainty in the net fluxes was difficult to calculate as some flux estimates were reported with standard deviations and other flux estimates only had minimum (min) and maximum (max) values (or 5^{th} and 95^{th} quantiles). For this reason we converted all standard deviations to a 5^{th} and 95^{th} quantiles using the equations; min = mean-1.645*sd; max = mean+1.645*sd. We then produced a min

and max net flux estimate by summing across these min and max values. When summing across positive and negative fluxes we summed the smallest fluxes, not the smallest numbers. For example, if the min NPP estimate was -8.18 and the max NPP estimate was -17.44 PgC, and the min Rh was 4.8 and the max Rh was 17.2 we summed -8.18 and 4.8 and -17.44 and 17.2. This is still a very crude way of assessing uncertainty and results in very large uncertainty values, but until we have more data on all fluxes it is the best uncertainty estimates we are able to provide at present.

Total CH_4 fluxes for Africa over the RECCAP2 period amount to 78.453 (36.665/59.677) $TgCyr^{-1}$. This BU estimate is very close to the TD estimate of 78.02 ± 3.88 (73.04/82.9) from the atmospheric inversion models. An estimate of 66 ± 35 $TgCH_4yr^{-1}$ was reported for RECCAP1 (Valentini et al. 2014). For N_2O, the RECCAP2 BU estimate of 1.81 (1.716/2.239) TgN_2O^{-1} is much lower than the estimate from the atmospheric inversions at 5.401 ± 0.22 (5.165/5.668). The RECCAP1 estimate was 3.3 ± 1.3 TgN_2Oyr^{-1}. As the large majority of N_2O emissions for Africa are from agricultural sources we would expect this flux to be increasing over time. Given the lack of certain component fluxes in our bottom-up estimates and the large uncertainty associated with our estimates, a considerable effort should be directed at improving observations and estimates for CH_4 and N_2O fluxes in Africa.

Considering the carbon in CO_2 and CH_4, we find that the BU approach estimates Africa to contribute 0.553 (-1.35/2.974) $PgCyr^{-1}$ to the global carbon cycle when we include non-terrestrial fluxes such as fossil fuels. Within this BU net carbon balance, terrestrial fluxes contribute 0.162 (-1.793/2.633) $PgCyr^{-1}$ with the rest being produced through anthropogenic emissions from fossil fuels and agriculture. However, the TD approaches estimate a much lower African contribution at 0.169 ± 0.27 (-0.015/1.616). Similarly, the calculated balance of fluxes from all three gases (in CO_2 equivalents) add to a total of 5.518 (-2.666/12.859) $PgCO_2eq\ yr^{-1}$ of which NEE contributes 2.585 (-5.899/10.225) $PgCO_2eq\ yr^{-1}$ for the BU approaches. The TD approaches estimate the African contribution of GHG emissions at 3.449 (2.614/4.287) $PgCO_2eq\ yr^{-1}$. The estimate for RECCAP1 (Valentini et al. 2014) was −2.66±4.28, but they did not include key aquatic fluxes which are significant contributions. The differences between the estimates from the BU and TD approaches is not unexpected as BU approaches often omit some flux components due to the challenges in observation and lack of data. In particular, the coastal ocean margin sink (Kwon et al., 2021) could not accurately be quantified so was omitted from the final budget, and models of above and below ground biomass change require further validation. The large uncertainty values of the TD approaches are also a consequence of the sparse surface observations which makes it difficult to constrain the inversion models.

Nevertheless, we find increasing trends of carbon and GHG emissions in the net balance estimates from both BU and TD approaches. Given the large uncertainties associated with these balances, it is difficult to definitively state that Africa is a source of carbon emissions, although it does appear to be likely. If we consider the contribution of N_2O and CH_4 in the total GHG net emission estimate, Africa

1 does however categorise as a net source. Certainly, we do see that Africa's carbon and GHG budget
2 remains close to carbon neutral and still contributes a small percentage to the global budget relative to
3 other regions. It is however concerning that the sink capacity in Africa is decreasing.

Table 17. Synthesis of the estimates (with uncertainties) and trends of GHG and carbon stocks (Pg) and fluxes (Pg yr^{-1}) for Africa over the RECCAP2 period (specific periods depicted by footnotes). Estimate units for CH_4 and N_2O in blue italics are Tg yr^{-1}. Where more than one estimate is provided for a component the value considered as the "best estimate" was used for calculating the net balances and is provided in bold. The bottom-up NEP, NEE, NBP and top-down atmospheric inversion estimates are highlighted in light grey.

	CO_2	CH_4	N_20	Carbon Budget		GHG budget (CO_2 equivalents)	
CARBON STOCKS				**Estimate (PgC)**	**Trend ($PgCyr^{-1}$)**		
Above ground biomass:							
Satellite based models [a]				**84 (71/95)**			
TRENDY model ensemble [a]				56 (48/64)			
aDGVM [c]				59.54			
Belowground biomass: Peat				36.9	-0.012		
Belowground biomass: Soils							
Soilgrids [b]				**87.7 (77/99)**			
TRENDY model ensemble [a]				148 ± 60			
aDGVM [c]				76.77			
Total Carbon stocks				208.6			
GHG FLUXES	**Estimate ($PgCO_2$ yr^{-1})**	**Estimate ($TgCH_4$ yr^{-1})**	**Estimate (TgN_2O yr^{-1})**	**Estimate (PgC yr^{-1})**	**Trend ($PgCyr^{-1}$)**	**Estimate ($PgCO_2eq$ yr^{-1})**	**Trend ($TgCO_2eq$ yr^{-1})**
GPP:							
Satellite based models [d]	-90.457 ± 9.02 (-105.295/-75.619)			-24.67 ± 2.46 (-28.717/-20.623)	-0.032	-90.457 (-105.295/-75.619)	-0.117
TRENDY model ensemble [a]	-103.039 ± 12.444 (-123.51/-82.568)			-28.102 ± 3.394 (-33.685/-22.519)	-0.094	-103.039 (-123.51/-82.568)	-0.345
aDGVM [c]	-49.17 (-49.17/-49.17)			-13.41 (-13.41/-13.41)	-0.114	-49.17 (-49.17/-49.17)	-0.418

Autotrophic respiration (Ra):							
TRENDY model ensemble [a]	56.082 ± 9.939 (39.732/72.432)			15.295 ± 2.711 (10.836/19.754)	0.051	56.082 (39.732/72.432)	0.186
aDGVM [c]	4.363 (4.363/4.363)			1.19 (1.19/1.19)	0.015	4.363 (4.363/4.363)	0.055
NPP:							
TRENDY model ensemble [a]	**-46.957 ± 10.322 (-63.936/-29.978)**			**-12.807 ± 2.815 (-17.437/-8.176)**	**-0.043**	**-46.957 (-63.936/-29.978)**	**-0.159**
aDGVM [c]	-44.807 (-44.807/-44.807)			-12.22 (-12.22/-12.22)	-0.063	-44.807 (-44.807/-44.807)	-0.231
Heterotrophic respiration (Rh):							
TRENDY model ensemble [a]	**40.436 ± 13.861 (17.635/63.238)**			**11.028 ± 3.78 (4.809/17.247)**	**0.025**	**40.436 (17.635/63.238)**	**0.092**
aDGVM [c]	32.34 (32.34/32.34)			8.82 (8.82/8.82)	0.051	32.34 (32.34/32.34)	0.187
Wild fire emissions:							
FREMv2.1 [a]	**3.25 (3.25/5.475)**	***6.792 (4.858/9.083)***	***0.085 (0.085/0.422)***	**0.953 ± 0.113 (0.953/1.595)**	**-0.011**	**3.433 (3.381/5.72)**	
TRENDY model ensemble [a]	3.154 ± 2.085 (-0.275/6.584)			0.86 ± 0.569 (-0.075/1.796)	-0.002	3.154 (-0.275/6.584)	
aDGVM [c]	4.217			1.15 (1.15/1.15)		4.217	
Land use change emissions:							
TRENDY model ensemble [a]				**0.476 ± 0.15 (0.229/0.723)**		**1.746 (0.841/2.651)**	
NET ECOSYSTEM PRODUCTION	-1.525 (-8.252/7.428)	*6.792 (4.858/9.083)*	*0.085 (0.085/0.422)*	-0.349 (-2.184/2.128)		-1.318 (-8.098/7.788)	
Biofuel emissions [a]	0.905 ± 0.165 (0.634/1.176)			0.247 ± 0.045 (0.173/0.321)	0.005	0.905 (0.634/1.176)	
Crop trade fluxes [a]	0.109 ± 0.047 (0.032/0.185)			0.03 ± 0.013 (0.009/0.051)		0.109 (0.032/0.185)	

Wood trade fluxes [a]	0 ± 0.005 (-0.008/0.008)			0 ± 0.001 (-0.002/0.002)	0 (-0.008/0.008)	
Lateral fluxes (aquatic) [a]	-0.192 (-0.192/-0.650)			-0.052 (-0.052/-0.177)	-0.192 (-0.192/-0.650)	
Aquatic atmospheric fluxes [a]	1.106 (0.872/1.349)	*8.988 (7.371/10.922)*	*0.027 (0.02/0.032)*	0.308 (0.245/0.368)	1.356 (1.077/1.652)	
Organic C burial [a] (freshwater/coastal)	-0.153 (-0.045/-0.233)			-0.042 (-0.012/-0.064)	-0.153 (-0.045/-0.233)	
Geological fluxes [a]	0.018 (0.004/0.033)	*1.014 (1.014/1.014)*		0.006 (0.002/0.01)	0.046 (0.031/0.06)	
Termites [a]		*1.397 (1.305/1.489)*		0.001 (0.001/0.001)	0.038 (0.035/0.04)	
Herbivores [a]		*17.623 (9.185/21.65)*		0.013 (0.007/0.016)	0.476 (0.248/0.585)	10.8
NET ECOSYSTEM EXCHANGE	0.269 (-7.601/9.942)	*35.814 (23.734/44.159)*	*0.112 (0.105/0.453)*	0.162 (-1.793/2.633)	2.585 (-5.899/10.225)	
Fossil fuels [a]	1.277 ± 0.107 (1.101/1.453)	*14.219 ± 0.786 (12.926/15.511)*	*0.301 ± 0.004 (0.294/0.308)*	0.359 ± 0.03 (0.31/0.408)	1.743 (1.531/1.956)	
Bunkers [a]	0.042 ± 0.002 (0.039/0.044)	*0.001 ± 0 (0.001/0.001)*	*0.001 ± 0 (0.001/0.001)*	0.011 ± 0 (0.011/0.012)	0.042 (0.039/0.045)	
Agriculture [a]		*22.464 ± 1.071 (20.703/24.225)*	*1.331 ± 0.045 (1.258/1.405)*	0.017 ± 0.001 (0.016/0.018)	0.97 (0.902/1.038)	
Waste [a]		*5.956 ± 0.329 (5.415/6.496)*	*0.065 ± 0.004 (0.058/0.072)*	0.004 (0.004/0.005)	0.179 (0.162/0.195)	
NET BOTTOM-UP TOTAL (NBP)	1.588 (-6.461/11.439)	*78.453 (36.665/59.677)*	*1.81 (1.716/2.239)*	0.553 (-1.35/2.974)	5.518 (-2.666/12.859)	
ATMOSPHERIC INVERSIONS (TOP-DOWN)	0.403 ± 0.99 (-0.257/1.063) [a]	*78.02 ± 3.88 (73.04/82.9)* [e]	*5.401 ± 0.22 (5.165/5.668)* [f]	0.169 ± 0.27 (-0.015/1.616)	3.984 (3.126/4.849)	

[a] 2010-2019 [b] 2009-2019 [c] 2009-2018 [d] 2009-2015 [e] 2009-2017 [f] 2009-2016

1

4. Conclusion

From a global perspective, Africa is important due to its size and potential for climate change mitigation through assumed increases of its carbon stocks. However, given the high anthropogenic pressure through rapid population growth that catalyses energy demand and land transformation, Africa is more likely to increase its relative contribution to global GHG emissions. This is evident from our synthesis that shows a decrease in the sink capacity of the continent, largely due to the contributions of land use and fossil fuel emissions. Increasing productivity trends due to CO_2 fertilisation, intentional afforestation (or reforestation) and widespread woody encroachment of open savanna ecosystems can be contested given our large range of above-ground biomass estimates. We require massive effort to reduce uncertainties through increasing the resolution of Africa-specific observations both spatially and temporally, and we need to develop models that account for the unique functioning of African ecosystems.

Land use change emissions in Africa is significant (0.51 ± 0.10 $PgCyr^{-1}$ in RECCAP1 and 0.476 ± 0.15 $PgCyr^{-1}$ in RECCAP2 - although methods differ widely) and still contributes slightly more than fossil fuels (0.359 ± 0.03) to the net CO_2 balance. This key component requires more directive attention because even with the availability of novel state-of-the-art satellite products, categorisation of land use and land cover is still coarse, irregular and largely difficult to verify. Apart from the spatial variability in land use pressure across ecoregions, inter-annual variability due to seasonal fluctuations and periodic climatic oscillations also play a large role in the year-to-year sink:source dynamic.

As one of the important fluxes in Africa, fire contributed between 46% and 65% to the global fire emission estimate. Although we have shown that wildfire emissions decreased from the RECCAP1 period, the concern remains that much of this decrease is a consequence of land conversion that manifests as an alternative source of GHG emissions to the atmosphere. Fire is a process that maintains functionality in a large proportion of Africa's ecosystems (e.g. grasslands and savannas) and its importance can therefore not be underestimated. Moreover, until we have more certainty on the soil carbon responses to changes in tree cover, fire, and grazing, it would be premature to draw conclusions regarding the carbon cycle implications of reduced fire. Stable soil carbon reserves can be lost when woody species spread into grasslands (Jackson et al., 2017; Mureva et al., 2018) and therefore although reduced fire is likely to increase above-ground carbon stores, the net effect might not be increased sink capacity. The TRENDY models all predict large increases in soil carbon reserves in the past few decades, but the causes of this are unclear, and should be further investigated.

For this synthesis, we made a concerted attempt to calculate lateral fluxes, both from crop and wood trade, and from rivers. However, much of the data is based on coarse methods that used tier 1 inventory data and/or taken from global models with insufficient Africa-specific observation data. Although lateral trade fluxes represent a relatively small contribution to the net estimates, future efforts should be directed at improved methodology and the inclusion of embodied carbon in products. Similarly for carbon transport in rivers, we advocate for increased observations and empirical studies that are specific to Africa.

To conclude, we show that Africa's sink capacity is decreasing and that the continent most likely switched from a small net sink to a small net source during the 2010-2019 period. Although we have improved many of the component estimates since the previous RECCAP period, we still have large uncertainties in our estimates. What is clear is that Africa has an increasing GHG emissions trend and it deviates from the mitigation aims of the Paris Agreement towards net-zero emissions. Forecasts of a growing population that is associated with increasing emissions from fossil fuel burning and land conversion will inevitably increase Africa's relative contribution to the global GHG estimates in the next decade. This may further be exacerbated by the lack of actionable policy and increasing socio-economic challenges that will likely multiply as climate change continues to impact the region. We suggest a directed attempt to increase the GHG observation network of Africa for all BU components of the GHG budget, but especially with regard to land use change and biomass estimates. Importantly, protocol for accountability within national pledges should be accompanied by enabling African countries to observe and report more consistently in a standardised way for centralisation of data in inventories.

The information from this African budget is key to assessing which aspects of the carbon cycle are most important to be managed, and what sorts of management is possible in the quest to achieve net zero. Shifts to C-neutral energy sources can potentially remove up to 30% (1.743 (1.531/1.956) $PgCO_2eq\ yr^{-1}$) of the current anthropogenic emissions but emissions from land use change (1.746 (0.841/2.651) $PgCO_2eq\ yr^{-1}$) are harder to reduce. Both agricultural intensification, and expansion of agricultural land will continue to increase GHG fluxes in the short term, and the impact on the GHG budget depends on the degree to which climate-smart agricultural practices can be rolled out in different contexts.

As natural ecosystems are increasing their C-sink capacity, and currently more than compensating for the land use change emissions (CO_2 fertilisation estimated as -2.02 +- 0.88 $PgCO_2eq\ yr^{-1}$ by the TRENDY model ensemble) there is hope that nature-positive investments in Africa can help balance the global GHG budget. The IPCC AR6 scenarios for limiting warming to 1.5 degrees include substantial carbon-capture in African ecosystems; 2.3 Pg annually by 2050, involving over 700 million ha of land (Forster et

al. 2018). Key fluxes in this budget that are targeted are the fuelwood emissions (0.91 $PgCO_2eq\ yr^{-1}$), and the above-ground biomass (highly uncertain), as well as climate-smart agricultural practices. There is no evidence yet that this is possible within the socio-ecological context, with evidence emerging that estimates of above-ground biomass increases are unrealistic, and some will have negative biodiversity and social outcomes (Bond et al., 2019; Armani et al. 2022). This RECCAP2 GHG budget sets a baseline against which to assess the effectiveness of policies, and highlights the key fluxes that need better quantification to support financing these interventions, and assessing their consequences.

A key flux highlighted here is the 0.48 (0.248/0.585) $PgCO_2eq\ yr^{-1}$ contributed by livestock methane emissions. Our paper demonstrates how sensitive this value is to incorrect emissions factors and to varying livestock production systems, and highlights that there is a growing body of evidence on the continent to enable better parameterisation of this important flux. Key also to note that only 60% of this methane flux represents a net increase above what would have been emitted by the wildlife of Africa before they were replaced with livestock (Hempson et al., 2017). Options for reducing the livestock methane flux in African ecosystems need to be sensitive to the social contexts involved, but policies enabling mixed livestock-wildlife systems might prove important.

Currently the ability to accurately monitor C stock changes at large scales in Africa is limited, as the remotely sensed datasets have not been well parameterised for these ecosystems. This will improve rapidly due to private-public partnerships as C offset projects are scrutinized and verification procedures provide the motivation for improved C monitoring. Soil carbon stocks likewise, need attention in the DGVM modelling community. Again, with better quantification it will be easier to access funding to drive ecosystem-based mitigation activities.

Given that Africa currently is almost certainly a net source of GHG emissions, it would be unwise to presume that this continent can help offset emissions in other regions, but there is huge opportunity to invest in ways to help African countries to follow nature-supporting, rather than nature-eroding development pathways, and to remain carbon neutral.

Acknowledgments, Samples, and Data

YE and SA was funded by Oppenheimer Generations Research and Conservation: the Future Ecosystems for Africa Program. TT was funded by the Swedish National Space Agency (Dnr: 2021-00144; 2021-00111), FORMAS (Dnr. 2021-00644) and the EU-Aid funded CASSECS Project (Dnr:

FOOD/2019/410-169). Ronny Lauerwald acknowledges funding from French state aid, managed by ANR under the "Investissements d'avenir" programme (ANR-16-CONV-0003). SL was funded by South African Research Chair Initiative (SARChl) (# 64796). Casey Ryan was funded by the SECO project (Dnr: NE/T01279X/1). Nicola Stevens was funded by Trapnell Fund, Linacre College – Oxford.

References

Ahlström, A., Raupach, M. R., Schurgers, G., Smith, B., Arneth, A., Jung, M., et al. (2015). The dominant role of semi-arid ecosystems in the trend and variability of the land CO_2 sink. *Science*, *348*(6237), 895–899. https://doi.org/10.1126/science.aaa1668

Ahmed, B. M., Nkunika, P. O. Y., Sileshi, G. W., French, J. R., Nyeko, P., & Jain, S. (2011). Potential impact of climate change on termite distribution in Africa. *British Journal of Environment and Climate Change*, *1*, 172–189. Retrieved from https://api.semanticscholar.org/CorpusID:55567254

Amos. 1999. The role of wood energy in Africa. FAO. Rome.

Andela, N., Morton, D. C., Giglio, L., Chen, Y., van der Werf, G. R., Kasibhatla, P. S., et al. (2017). A human-driven decline in global burned area. *Science*, *356*(6345), 1356–1362.

Armani, M., Asefa, M., Zakari, S. & Agyekum, E.O. 2022. Technical report on enhancing climate change adaptation and mitigation actions on land in Africa. Archibald, S.A., Pereira, L.M., Coetzer, K.L., editors. Technical Report. Future Ecosystems for Africa (FEFA), University of the Witwatersrand, Johannesburg, 92pp.

Avitabile, V., Herold, M., Heuvelink, G. B. M., Lewis, S. L., Phillips, O. L., Asner, G. P., et al. (2016). An integrated pan-tropical biomass map using multiple reference datasets. *Global Change Biology*, *22*(4), 1406–1420. https://doi.org/https://doi.org/10.1111/gcb.13139

Baccini, A., Goetz, S. J., Walker, W. S., Laporte, N. T., Sun, M., Sulla-Menashe, D., et al. (2012). Estimated carbon dioxide emissions from tropical deforestation improved by carbon-density maps. *Nature Climate Change*, *2*(3), 182–185. https://doi.org/10.1038/nclimate1354

Baccini, A., Walker, W., Carvalho, L., Farina, M., Sulla-Menashe, D., & Houghton, R. A. (2017). Tropical forests are a net carbon source based on aboveground measurements of gain and loss. *Science*, *358*(6360), 230–234. https://doi.org/10.1126/science.aam5962

Bailis, R., Drigo, R., Ghilardi, A., & Masera, O. (2015). The carbon footprint of traditional woodfuels. *Nature Climate Change*, *5*(3), 266–272. https://doi.org/10.1038/nclimate2491

Bergamaschi, P., Krol, M., Meirink, J. F., Dentener, F., Segers, A., Van Aardenne, J., et al. (2010). Inverse modeling of European CH4 emissions 2001-2006. *Journal of Geophysical Research Atmospheres*, *115*(22), 1–18. https://doi.org/10.1029/2010JD014180

Bergamaschi, P., Houweling, S., Segers, A., Krol, M., Frankenberg, C., Scheepmaker, R. A., et al. (2013). Atmospheric CH4 in the first decade of the 21st century: Inverse modeling analysis using SCIAMACHY satellite retrievals and NOAA surface measurements. *Journal of Geophysical Research Atmospheres*, *118*(13), 7350–7369. https://doi.org/10.1002/jgrd.50480

Bergamaschi, Peter, Karstens, U., Manning, A. J., Saunois, M., Tsuruta, A., Berchet, A., et al. (2018). Inverse modelling of European CH4 emissions during 2006-2012 using different inverse models and reassessed atmospheric observations. *Atmospheric Chemistry and Physics*, *18*(2), 901–920. https://doi.org/10.5194/acp-18-901-2018

Blamey, R. C., Kolusu, S. R., Mahlalela, P., Todd, M. C., & Reason, C. J. C. (2018). The role of regional circulation features in regulating El Niño climate impacts over southern Africa: A comparison of the 2015/2016 drought with previous events. *International Journal of Climatology*, *38*(11), 4276–4295. https://doi.org/https://doi.org/10.1002/joc.5668

Boden, T. A., Marland, G., and Andres, R. J.: Global, Regional, and National Fossil-Fuel CO2 Emissions, Oak Ridge National Laboratory, U.S. Department of Energy, Oak Ridge, Tenn., USA, 2013.

Bombelli, A., Henry, M., Castaldi, S., Adu-Bredu, S., Arneth, A., Grandcourt, A. De, et al. (2009). The Sub-Saharan Africa carbon balance The Sub-Saharan Africa carbon balance, an overview The Sub-Saharan Africa carbon balance. Retrieved from www.biogeosciences-discuss.net/6/2085/2009/

Bond, W. J., Stevens, N., Midgley, G. F., & Lehmann, C. E. R. (2019). The Trouble with Trees: Afforestation Plans for Africa. *Trends in Ecology & Evolution*, *34*(11), 963–965. https://doi.org/10.1016/j.tree.2019.08.003

Borges, A. V., Deirmendjian, L., Bouillon, S., Okello, W., Lambert, T., Roland, F. A. E. E., et al. (2022). Greenhouse gas emissions from African lakes are no longer a blind spot. *Sci. Adv*, *8*(25), 8716. https://doi.org/10.1126/sciadv.abi8716

Borges, A. V, Darchambeau, F., Teodoru, C. R., Marwick, T. R., Tamooh, F., Geeraert, N., et al. (2015). Globally significant greenhouse-gas emissions from African inland waters. *Nature Geoscience*, *8*(8), 637–642. https://doi.org/10.1038/ngeo2486

Bouvet, A., Mermoz, S., Le Toan, T., Villard, L., Mathieu, R., Naidoo, L., & Asner, G. P. (2018). An above-ground biomass map of African savannahs and woodlands at 25 m resolution derived from ALOS PALSAR. *Remote Sensing of Environment*, *206*(November 2017), 156–173. https://doi.org/10.1016/j.rse.2017.12.030

Brandt, M., Yue, Y., Wigneron, J. P., Tong, X., Tian, F., Jepsen, M. R., et al. (2018). Satellite-Observed Major Greening and Biomass Increase in South China Karst During Recent Decade. *Earth's Future*, *6*(7), 1017–1028. https://doi.org/10.1029/2018EF000890

Brauman, A., Doré, J., Eggleton, P., Bignell, D., Breznak, J. A., & Kane, M. D. (2001). Molecular phylogenetic profiling of prokaryotic communities in guts of termites with different feeding habits. *FEMS Microbiology Ecology*, *35*(1), 27–36. https://doi.org/10.1111/j.1574-6941.2001.tb00785.x

Broadhead, J., Bahdon, J., Whiteman, A. (2001). Past trends and future prospects for the utilization of wood for energy (Annex 1 and Annex 2), Global Forest Products Outlook Study (GFPOS). FAO 2001.

Brune, A. (2014). Symbiotic digestion of lignocellulose in termite guts. *Nature Reviews. Microbiology*, *12*(3), 168–180. https://doi.org/10.1038/nrmicro3182

Chang, J., Peng, S., Yin, Y., Ciais, P., Havlik, P., & Herrero, M. (2021). The Key Role of Production Efficiency Changes in Livestock Methane Emission Mitigation. *AGU Advances*, *2*(2), 1–16. https://doi.org/10.1029/2021av000391

Chevallier, F., Fisher, M., Peylin, P., Serrar, S., Bousquet, P., Bréon, F.-M., et al. (2005). Inferring CO2 sources and sinks from satellite observations: Method and application to TOVS data. *Journal of Geophysical Research: Atmospheres*, *110*(D24). https://doi.org/https://doi.org/10.1029/2005JD006390

Chevallier, F., Remaud, M., O'Dell, C. W., Baker, D., Peylin, P., & Cozic, A. (2019). Objective evaluation of surface- and satellite-driven carbon dioxide atmospheric inversions. *Atmospheric Chemistry and Physics*, *19*(22), 14233–14251. https://doi.org/10.5194/acp-19-14233-2019

Ciais, P, Bombelli, A., Williams, M., Piao, S. L., Chave, J., Ryan, C. M., et al. (2011). The carbon balance of Africa: synthesis of recent research studies. *Philosophical Transactions. Series A, Mathematical, Physical, and Engineering Sciences*, *369*(1943), 2038–2057. https://doi.org/10.1098/rsta.2010.0328

Ciais, Philippe, Bastos, A., Chevallier, F., Lauerwald, R., Poulter, B., Canadell, P., et al. (2022). Definitions and methods to estimate regional land carbon fluxes for the second phase of the REgional Carbon Cycle Assessment and Processes Project (RECCAP-2). *Geoscientific Model Development*, *15*(3), 1289–1316. https://doi.org/10.5194/gmd-15-1289-2022

Dargie, G. C., Lewis, S. L., Lawson, I. T., Mitchard, E. T. A., Page, S. E., Bocko, Y. E., & Ifo, S. A. (2017). Age, extent and carbon storage of the central Congo Basin peatland complex. *Nature*, *542*(7639), 86–90. https://doi.org/10.1038/nature21048

Diouf, A. A., Brandt, M., Verger, A., El Jarroudi, M., Djaby, B., Fensholt, R., et al. (2015). Fodder biomass

monitoring in Sahelian rangelands using phenological metrics from FAPAR time series. *Remote Sensing*, *7*(7), 9122–9148. https://doi.org/10.3390/rs70709122

Dong, H., Mangino, J., McAllister, T. A., Hatfield, J. L., Johnson, D. E., Bartram, D., et al. (2006). 2006 IPCC Guidelines for National Greenhouse Gas inventories - Chapter 10: Emissions from livestock and manure management.

Etiope, G., Ciotoli, G., Schwietzke, S., & Schoell, M. (2019). Gridded maps of geological methane emissions and their isotopic signature. *Earth System Science Data*, *11*(1). https://doi.org/10.5194/essd-11-1-2019

Ernst, Y. & Scholes, R.J. (2023). Scholes African Ecoregions (Version 1) [Data set]. Zenodo. https://doi.org/10.5281/zenodo.8217315

FAO. 2010. Criteria and indicators for sustainable woodfuels. FAO Forestry Paper No. 160. Rome

Feng, L., Palmer, P. I., Parker, R. J., Deutscher, N. M., Feist, D. G., Kivi, R., et al. (2016). Estimates of European uptake of CO_2 inferred from GOSAT X_{CO2} retrievals: sensitivity to measurement bias inside and outside Europe. *Atmospheric Chemistry and Physics*, *16*(3), 1289–1302. https://doi.org/10.5194/acp-16-1289-2016

Feng, X., Fu, B., Zhang, Y., Pan, N., Zeng, Z., Tian, H., et al. (2021). Recent leveling off of vegetation greenness and primary production reveals the increasing soil water limitations on the greening Earth. *Science Bulletin*, *66*(14), 1462–1471. https://doi.org/https://doi.org/10.1016/j.scib.2021.02.023

Forster, P., D. Huppmann, E. Kriegler, L. Mundaca, C. Smith, J. Rogelj, & Seferian, R. (2018). *Mitigation Pathways Compatible with 1.5°C in the Context of Sustainable Development Supplementary Material*. In: Global Warming of 1.5°C. An IPCC Special Report on the impacts of global warming of 1.5°C above pre-industrial levels and related global greenhouse gas emission pathways, in the context of strengthening the global response to the threat of climate change, sustainable development, and efforts to eradicate poverty [Masson-Delmotte, V., P. Zhai, H.-O. Portner, D. Roberts, J. Skea, P.R. Shukla, A. Pirani, W. Moufouma-Okia, C. Pean, R. Pidcock, S. Connors, J.B.R. Matthews, Y. Chen, X. Zhou, M.I. Gomis, E. Lonnoy, T. Maycock, M. Tignor, and T. Waterfield (eds.)]. Available from https://www.ipcc.ch/sr15

Friedlingstein, P, O'Sullivan, M., Jones, M. W., Andrew, R. M., Hauck, J., Olsen, A., et al. (2020). Global Carbon Budget 2020. *Earth System Science Data*, *12*(4), 3269–3340. https://doi.org/10.5194/essd-12-3269-2020

Friedlingstein, Pierre, Jones, M. W., O'Sullivan, M., Andrew, R. M., Bakker, D. C. E., Hauck, J., et al. (2022). Global Carbon Budget 2021. *Earth System Science Data*, *14*(4), 1917–2005. https://doi.org/10.5194/essd-14-1917-2022

Gaubert, B, Stephens, B. B., Basu, S., Chevallier, F., Deng, F., Kort, E. A., et al. (2019). Global atmospheric GOSAT X_{CO2} inverse models converging on neutral tropical land exchange, but disagreeing on fossil fuel and atmospheric growth rate. *Biogeosciences*, *16*(1), 117–134. https://doi.org/10.5194/bg-16-117-2019

Gaubert, B, Stephens, B. B., Baker, D. F., Basu, S., Bertolacci, M., Bowman, K. W., et al. (2023). Neutral tropical African CO2 exchange estimated from aircraft and satellite observations. Retrieved from https://doi.org/10.22541/essoar.168167225.54628972/v1

Gloor, E., Wilson, C., Chipperfield, M. P., Chevallier, F., Buermann, W., Boesch, H., et al. (2018). Tropical land carbon cycle responses to 2015/16 El Niño as recorded by atmospheric greenhouse gas and remote sensing data. *Philosophical Transactions of the Royal Society B: Biological Sciences*, *373*(1760). https://doi.org/10.1098/rstb.2017.0302

Gomes, A. L., Revermann, R., Gonçalves, F. M. P., Lages, F., Aidar, M. P. M., Sanguino Mostajo, G. A., & Finckh, M. (2021). Suffrutex grasslands in south-central Angola: belowground biomass, root structure, soil characteristics and vegetation dynamics of the 'underground forests of Africa.' *Journal of Tropical Ecology*, *37*(3), 136–146. https://doi.org/10.1017/S0266467421000298

Goopy, J. P., Ndung'u, P. W., Onyango, A., Kirui, P., & Butterbach-Bahl, K. (2021). Calculation of new enteric methane emission factors for small ruminants in western Kenya highlights the heterogeneity of smallholder production systems. *Animal Production Science*, *61*(6), 602–612. https://doi.org/10.1071/AN19631

Hantson, S., Arneth, A., Harrison, S. P., Kelley, D. I., Colin Prentice, I., Rabin, S. S., et al. (2016). The status and challenge of global fire modelling. *Biogeosciences*, *13*(11), 3359–3375. https://doi.org/10.5194/bg-13-3359-2016

Hartmann, J., Jansen, N., Dürr, H. H., Kempe, S., & Köhler, P. (2009). Global CO2-consumption by chemical weathering: What is the contribution of highly active weathering regions? *Global and Planetary Change*, *69*(4), 185–194. https://doi.org/10.1016/j.gloplacha.2009.07.007

Hartmann, J., Lauerwald, R., & Moosdorf, N. (2014). A Brief Overview of the GLObal RIver Chemistry Database, GLORICH. *Procedia Earth and Planetary Science*, *10*, 23–27. https://doi.org/10.1016/j.proeps.2014.08.005

Hempson, G. P., Archibald, S., & Bond, W. J. (2017). The consequences of replacing wildlife with livestock in Africa. *Scientific Reports*, *7*(1), 1–10. https://doi.org/10.1038/s41598-017-17348-4

Hengl, T., Heuvelink, G. B. M., Kempen, B., Leenaars, J. G. B., Walsh, M. G., Shepherd, K. D., et al. (2015). Mapping soil properties of Africa at 250 m resolution: Random forests significantly improve current predictions. *PLoS ONE*, *10*(6), 1–26. https://doi.org/10.1371/journal.pone.0125814

Hengl, T., Mendes de Jesus, J., Heuvelink, G. B. M., Ruiperez Gonzalez, M., Kilibarda, M., Blagotić, A., et al. (2017). SoilGrids250m: Global gridded soil information based on machine learning. *PloS One*, *12*(2), e0169748. https://doi.org/10.1371/journal.pone.0169748

Herrero, M., Thornton, P. K., Kruska, R., & Reid, R. S. (2008). Systems dynamics and the spatial distribution of methane emissions from African domestic ruminants to 2030. *Agriculture, Ecosystems & Environment*, *126*(1), 122–137. https://doi.org/https://doi.org/10.1016/j.agee.2008.01.017

Höglund-Isaksson, L., Gómez-Sanabria, A., Klimont, Z., Rafaj, P., & Schöpp, W. (2020). Technical potentials and costs for reducing global anthropogenic methane emissions in the 2050 timeframe –results from the gains model. *Environmental Research Communications*, *2*(2). https://doi.org/10.1088/2515-7620/ab7457

Hubau, W., Lewis, S. L., Phillips, O. L., Affum-Baffoe, K., Beeckman, H., Cuní-Sanchez, A., et al. (2020). Asynchronous carbon sink saturation in African and Amazonian tropical forests. *Nature*, *579*(7797), 80–87. https://doi.org/10.1038/s41586-020-2035-0

Hunt, J. A., Zafu, A., Mather, T. A., Pyle, D. M., & Barry, P. H. (2017). Spatially Variable CO2 Degassing in the Main Ethiopian Rift: Implications for Magma Storage, Volatile Transport, and Rift-Related Emissions. *Geochemistry, Geophysics, Geosystems*, *18*(10), 3714–3737. https://doi.org/10.1002/2017GC006975

IPCC. (2019). Volume 4: Agriculture, Forestry and Other Land Use. Chapter 10: Emissions form Livestock and Manure Management. *2019 Refinement to the 2006 IPCC Guidelines for National Greenhouse Gas InventorieS*, *4*, 209.

IPCC. (2021). *Climate Change 2021: The Physical Science Basis. Contribution of Working Group I to the Sixth Assessment Report of the Intergovernmental Panel on Climate Change* [Masson-Delmotte, V., P. Zhai, A. Pirani, S.L. Connors, C. Péan, S. Berger, N. Caud, Y. Chen, L. Goldfarb, M.I. Gomis, M. Huang, K. Leitzell, E. Lonnoy, J.B.R. Matthews, T.K. Maycock, T. Waterfield, O. Yelekçi, R. Yu, and B. Zhou (eds.)]. Cambridge University Press, Cambridge, United Kingdom and New York, NY, USA, In press, doi:10.1017/9781009157896.

IEA (2022). World Energy Statistics. https://www.iea.org/data-and-statistics/data-product/world-energy-statistics

IEA (2023). Greenhouse Gas Emissions from Energy Highlights. https://www.iea.org/data-and-statistics/data-product/greenhouse-gas-emissions-from-energy-highlights

Jackson, R. B., Lajtha, K., Crow, S. E., Hugelius, G., Kramer, M. G., & Piñeiro, G. (2017). The Ecology of Soil Carbon: Pools, Vulnerabilities, and Biotic and Abiotic Controls. *Annual Review of Ecology, Evolution, and Systematics*, *48*(1), 419–445. https://doi.org/10.1146/annurev-ecolsys-112414-054234

Joosten, H. (2009). The Global Peatland CO2 Picture. *Africa*, 11.

Kirschke, S., Bousquet, P., Ciais, P., Saunois, M., Canadell, J. G., Dlugokencky, E. J., et al. (2013). Three decades

of global methane sources and sinks. *Nature Geoscience*, *6*(10), 813–823. https://doi.org/10.1038/ngeo1955

Kwon, E. Y., DeVries, T., Galbraith, E. D., Hwang, J., Kim, G., & Timmermann, A. (2021). Stable Carbon Isotopes Suggest Large Terrestrial Carbon Inputs to the Global Ocean. *Global Biogeochemical Cycles*, *35*(4), 1–25. https://doi.org/10.1029/2020GB006684

Lacroix, F., Ilyina, T., & Hartmann, J. (2020). Oceanic CO2 outgassing and biological production hotspots induced by pre-industrial river loads of nutrients and carbon in a global modeling approach. *Biogeosciences*, *17*(1), 55–88. https://doi.org/10.5194/bg-17-55-2020

Lasslop, G., Hantson, S., Harrison, S. P., Bachelet, D., Burton, C., Forkel, M., et al. (2020). Global ecosystems and fire: Multi-model assessment of fire-induced tree-cover and carbon storage reduction. *Global Change Biology*, *26*(9), 5027–5041. https://doi.org/https://doi.org/10.1111/gcb.15160

Lauerwald, R., Allen, G. H., Deemer, B. R., Liu, S., Maavara, T., Raymond, P., et al. (2023). Inland Water Greenhouse Gas Budgets for RECCAP2: 2. Regionalization and Homogenization of Estimates. *Global Biogeochemical Cycles*, *37*(5), e2022GB007658. https://doi.org/https://doi.org/10.1029/2022GB007658

Lee, H., Muirhead, J. D., Fischer, T. P., Ebinger, C. J., Kattenhorn, S. A., Sharp, Z. D., & Kianji, G. (2016). Massive and prolonged deep carbon emissions associated with continental rifting. *Nature Geoscience*, *9*(2), 145–149. https://doi.org/10.1038/ngeo2622

Lewis, S. L., Lopez-Gonzalez, G., Sonké, B., Affum-Baffoe, K., Baker, T. R., Ojo, L. O., et al. (2009). Increasing carbon storage in intact African tropical forests. *Nature*, *457*(7232), 1003–1006. https://doi.org/10.1038/nature07771

Liu, J., Baskaran, L., Bowman, K., Schimel, D., Bloom, A. A., Parazoo, N. C., et al. (2021). Carbon Monitoring System Flux Net Biosphere Exchange 2020 (CMS-Flux NBE 2020). *Earth System Science Data*, *13*(2), 299–330. https://doi.org/10.5194/essd-13-299-2021

Liu, J., Bowman, K. W., Schimel, D. S., Parazoo, N. C., Jiang, Z., Lee, M., et al. (2017). Contrasting carbon cycle responses of the tropical continents to the 2015–2016 El Niño. *Science*, *358*(6360). https://doi.org/10.1126/science.aam5690

Liu, Y. Y., van Dijk, A. I. J. M., de Jeu, R. A. M., Canadell, J. G., McCabe, M. F., Evans, J. P., & Wang, G. (2015). Recent reversal in loss of global terrestrial biomass. *Nature Climate Change*, *5*(5), 470–474. https://doi.org/10.1038/nclimate2581

Lourenco, M., Fitchett, J. M., & Woodborne, S. (2022). Angolan highlands peatlands: Extent, age and growth dynamics. *Science of The Total Environment*, *810*, 152315. https://doi.org/https://doi.org/10.1016/j.scitotenv.2021.152315

Ludwig, W., Amiotte-Suchet, P., Munhoven, G., & Probst, J.-L. (1998). Atmospheric CO2 consumption by continental erosion: present-day controls and implications for the last glacial maximum. *Global and Planetary Change*, *16–17*, 107–120. https://doi.org/https://doi.org/10.1016/S0921-8181(98)00016-2

Macdonald, J. A., Jeeva, D., Eggleton, P., Davies, R., Bignell, D. E., Fowler, D., et al. (1999). The effect of termite biomass and anthropogenic disturbance on the CH4 budgets of tropical forests in Cameroon and Borneo. *Global Change Biology*, *5*(8), 869–879. https://doi.org/https://doi.org/10.1046/j.1365-2486.1999.00279.x

Maksyutov, S., Oda, T., Saito, M., Janardanan, R., Belikov, D., Kaiser, J. W., et al. (2021). Technical note: A high-resolution inverse modelling technique for estimating surface CO2 fluxes based on the NIES-TM-FLEXPART coupled transport model and its adjoint. *Atmospheric Chemistry and Physics*, *21*(2), 1245–1266. https://doi.org/10.5194/acp-21-1245-2021

Martens, C., Hickler, T., Davis-Reddy, C., Engelbrecht, F., Higgins, S. I., von Maltitz, G. P., et al. (2021). Large uncertainties in future biome changes in Africa call for flexible climate adaptation strategies. *Global Change Biology*, *27*(2), 340–358. https://doi.org/https://doi.org/10.1111/gcb.15390

McNicol, I. M., Ryan, C. M., & Mitchard, E. T. A. (2018). Carbon losses from deforestation and widespread degradation offset by extensive growth in African woodlands. *Nature Communications*, *9*(1), 3045. https://doi.org/10.1038/s41467-018-05386-z

Mendonça, R., Müller, R. A., Clow, D., Verpoorter, C., Raymond, P., Tranvik, L. J., & Sobek, S. (2017). Organic carbon burial in global lakes and reservoirs. *Nature Communications*, *8*(1). https://doi.org/10.1038/s41467-017-01789-6

Mokany, K., Raison, R. J., & Prokushkin, A. S. (2006). Critical analysis of root : shoot ratios in terrestrial biomes. *Global Change Biology*, *12*(1), 84–96. https://doi.org/https://doi.org/10.1111/j.1365-2486.2005.001043.x

Mostefaoui, M., Ciais, P., Mcgrath, M. J., Peylin, P., Prabir, K., & Ernst, Y. (2023). Greenhouse gas emissions and their trends over the last three decades across Africa, (July).

Mureva, A., Ward, D., Pillay, T., Chivenge, P., & Cramer, M. (2018). Soil Organic Carbon Increases in Semi-Arid Regions while it Decreases in Humid Regions Due to Woody-Plant Encroachment of Grasslands in South Africa. *Scientific Reports*, *8*(1), 1–12. https://doi.org/10.1038/s41598-018-33701-7

Ndung'u, P. W., Takahashi, T., du Toit, C. J. L., Robertson-Dean, M., Butterbach-Bahl, K., McAuliffe, G. A., et al. (2022). Farm-level emission intensities of smallholder cattle (Bos indicus; B. indicus–B. taurus crosses) production systems in highlands and semi-arid regions. *Animal*, *16*(1), 100445. https://doi.org/10.1016/j.animal.2021.100445

Nguyen, H. M., & Wooster, M. J. (2020). Remote Sensing of Environment Advances in the estimation of high Spatio-temporal resolution pan-African top-down biomass burning emissions made using geostationary fire radiative power (FRP) and MAIAC aerosol optical depth (AOD) data. *Remote Sensing of Environment*, *248*(July), 111971. https://doi.org/10.1016/j.rse.2020.111971

Niwa, Y., Tomita, H., Satoh, M., Imasu, R., Sawa, Y., Tsuboi, K., et al. (2017). A 4D-Var inversion system based on the icosahedral grid model (NICAM-TM 4D-Var v1.0)-Part 1: Offline forward and adjoint transport models. *Geoscientific Model Development*, *10*(3), 1157–1174. https://doi.org/10.5194/gmd-10-1157-2017

Ochiai, O., Poulter, B., Seifert, F. M., Ward, S., Jarvis, I., Whitcraft, A., et al. (2023). iScience ll Towards a roadmap for space-based observations of the land sector for the UNFCCC global stocktake. *ISCIENCE*, *26*(4), 106489. https://doi.org/10.1016/j.isci.2023.106489

Pachzelt, A., Forrest, M., Rammig, A., Higgins, S. I., & Hickler, T. (2015). Potential impact of large ungulate grazers on African vegetation, carbon storage and fire regimes. *Global Ecology and Biogeography*, *24*(9), 991–1002. https://doi.org/https://doi.org/10.1111/geb.12313

Palmer, P. I., Feng, L., Baker, D., Chevallier, F., Bösch, H., & Somkuti, P. (2019). Net carbon emissions from African biosphere dominate pan-tropical atmospheric CO2 signal. *Nature Communications*, *10*(1), 1–9. https://doi.org/10.1038/s41467-019-11097-w

Pan, S., Dangal, S. R. S., Tao, B., Yang, J., & Tian, H. (2015). Recent patterns of terrestrial net primary production in africa influenced by multiple environmental changes. *Ecosystem Health and Sustainability*, *1*(5), 1–15. https://doi.org/10.1890/EHS14-0027.1

Pandey, S., Houweling, S., Krol, M., Aben, I., Chevallier, F., Dlugokencky, E. J., et al. (2016). Inverse modeling of GOSAT-retrieved ratios of total column CH4 and CO2 for 2009 and 2010. *Atmospheric Chemistry and Physics*, *16*(8), 5043–5062. https://doi.org/10.5194/acp-16-5043-2016

Pelletier, J., Paquette, A., Mbindo, K., Zimba, N., Siampale, A., Chendauka, B., et al. (2018). Carbon sink despite large deforestation in African tropical dry forests (miombo woodlands). *Environmental Research Letters*, *13*(9), 94017. https://doi.org/10.1088/1748-9326/aadc9a

Peñuelas, J., Poulter, B., Sardans, J., Ciais, P., van der Velde, M., Bopp, L., et al. (2013). Human-induced nitrogen–phosphorus imbalances alter natural and managed ecosystems across the globe. *Nature Communications*, *4*(1), 2934. https://doi.org/10.1038/ncomms3934

Peters, G. P., Davis, S. J., & Andrew, R. (2012). A synthesis of carbon in international trade. *Biogeosciences*, *9*(8), 3247–3276. https://doi.org/10.5194/bg-9-3247-2012

Piao, S., Wang, X., Park, T., Chen, C., Lian, X., He, Y., et al. (2020). Characteristics, drivers and feedbacks of global greening. *Nature Reviews Earth & Environment*, *1*(1), 14–27. https://doi.org/10.1038/s43017-019-0001-x

Potapov, P., Li, X., Hernandez-Serna, A., Tyukavina, A., Hansen, M. C., Kommareddy, A., et al. (2021). Mapping global forest canopy height through integration of GEDI and Landsat data. *Remote Sensing of Environment*, *253*, 1–30. https://doi.org/10.1016/j.rse.2020.112165

Potapov, P., Hansen, M. C., Pickens, A., Hernandez-Serna, A., Tyukavina, A., Turubanova, S., et al. (2022). The Global 2000-2020 Land Cover and Land Use Change Dataset Derived From the Landsat Archive: First Results. *Frontiers in Remote Sensing*, *3*(April), 1–22. https://doi.org/10.3389/frsen.2022.856903

Poulter, B., Frank, D. C., Hodson, E. L., & Zimmermann, N. E. (2011). Impacts of land cover and climate data selection on understanding terrestrial carbon dynamics and the CO$_{2}$ airborne fraction. *Biogeosciences*, *8*(8), 2027–2036. https://doi.org/10.5194/bg-8-2027-2011

Ramo, R., Roteta, E., Bistinas, I., Van Wees, D., Bastarrika, A., Chuvieco, E., & Van der Werf, G. R. (2021). African burned area and fire carbon emissions are strongly impacted by small fires undetected by coarse resolution satellite data. *Proceedings of the National Academy of Sciences*, *118*(9).

Randerson, J. T., Van Der Werf, G. R., Giglio, L., Collatz, G. J., & Kasibhatla, P. S. (2017). Global Fire Emissions Database, Version 4.1 (GFEDv4). ORNL Distributed Active Archive Center. https://doi.org/10.3334/ORNLDAAC/1293

Räsänen, M., Vesala, R., Rönnholm, P., Arppe, L., Manninen, P., & Jylhä, M. (2023). Carbon dioxide and methane fluxes from mounds of African fungus-growing termites, 4029–4042.

Rödenbeck, C., Houweling, S., Gloor, M., & Heimann, M. (2003). CO2 flux history 1982–2001 inferred from atmospheric data using a global inversion of atmospheric transport. *Atmospheric Chemistry and Physics*, *3*(6), 1919–1964. https://doi.org/10.5194/acp-3-1919-2003

Rödenbeck, C., Zaehle, S., Keeling, R., & Heimann, M. (2018). How does the terrestrial carbon exchange respond to inter-annual climatic variations? A quantification based on atmospheric CO2 data. *Biogeosciences*, *15*(8), 2481–2498. https://doi.org/10.5194/bg-15-2481-2018

Rodríguez-Veiga, P., Wheeler, J., Louis, V., Tansey, K., & Balzter, H. (2017). Quantifying Forest Biomass Carbon Stocks From Space. *Current Forestry Reports*, *3*(1), 1–18. https://doi.org/10.1007/s40725-017-0052-5

Roteta, E., Bastarrika, A., Padilla, M., Storm, T., & Chuvieco, Ejrs. (2019). Development of a Sentinel-2 burned area algorithm: Generation of a small fire database for sub-Saharan Africa. *Remote Sensing of Environment*, *222*, 1–17.

Rouland, C., Brauman, A., Labat, M., & Lepage, M. (1993). Nutritional factors affecting methane emission from termites. *Chemosphere*, *26*(1), 617–622. https://doi.org/https://doi.org/10.1016/0045-6535(93)90447-D

Saatchi, S. S., Harris, N. L., Brown, S., Lefsky, M., Mitchard, E. T. A., Salas, W., et al. (2011). Benchmark map of forest carbon stocks in tropical regions across three continents. *Proceedings of the National Academy of Sciences*, *108*(24), 9899–9904. https://doi.org/10.1073/pnas.1019576108

Sankaran, M., Hanan, N. P., Scholes, R. J., Ratnam, J., Augustine, D. J., Cade, B. S., et al. (2005). Determinants of woody cover in African savannas. *Nature*, *438*(7069), 846–849. https://doi.org/10.1038/nature04070

Santoro, M., Cartus, O., Carvalhais, N., Rozendaal, D. M. A. A., Avitabile, V., Araza, A., et al. (2021). The global forest above-ground biomass pool for 2010 estimated from high-resolution satellite observations. *Earth System Science Data*, *13*(8), 3927–3950. https://doi.org/10.5194/essd-13-3927-2021

Sato, H., & Ise, T. (2012). Effect of plant dynamic processes on African vegetation responses to climate change: Analysis using the spatially explicit individual-based dynamic global vegetation model (SEIB-DGVM). *Journal of Geophysical Research: Biogeosciences*, *117*(G3). https://doi.org/https://doi.org/10.1029/2012JG002056

Saunois, M., R. Stavert, A., Poulter, B., Bousquet, P., G. Canadell, J., B. Jackson, R., et al. (2020). The global methane budget 2000-2017. *Earth System Science Data*, *12*(3), 1561–1623. https://doi.org/10.5194/essd-12-1561-2020

Scheiter, S., & Higgins, S. I. (2009). Impacts of climate change on the vegetation of Africa: an adaptive dynamic vegetation modelling approach. *Global Change Biology*, *15*(9), 2224–2246.

https://doi.org/https://doi.org/10.1111/j.1365-2486.2008.01838.x

Scholes, R. J., Archibald, S., & Maltitz, G. Von. (2011). Emissions from Fire in Sub-Saharan Africa: the Magnitude of Sources, Their Variability and Uncertainty.

Schuh, A. E., Jacobson, A. R., Basu, S., Weir, B., Baker, D., Bowman, K., et al. (2019). Quantifying the Impact of Atmospheric Transport Uncertainty on CO2 Surface Flux Estimates. *Global Biogeochemical Cycles*, *33*(4), 484–500. https://doi.org/10.1029/2018GB006086

Segers, A. & Houweling, S. (2018). Validation of the CH4 surface flux inversion - reanalysis 1990-2017, Copernicus Atmosphere Monitoring Service.

Song, X.-P., Hansen, M. C., Stehman, S. V, Potapov, P. V, Tyukavina, A., Vermote, E. F., & Townshend, J. R. (2018). Global land change from 1982 to 2016. *Nature*, *560*(7720), 639–643. https://doi.org/10.1038/s41586-018-0411-9

Stevens, N., Erasmus, B. F. N., Archibald, S., & Bond, W. J. (2016). Woody encroachment over 70 years in South African savannahs: overgrazing, global change or extinction aftershock? *Philosophical Transactions of the Royal Society of London. Series B, Biological Sciences*, *371*(1703). https://doi.org/10.1098/rstb.2015.0437

Syampungani, S., Geldenhuys, C. J., & Chirwa, P. W. (2016). Regeneration dynamics of miombo woodland in response to different anthropogenic disturbances: forest characterisation for sustainable management. *Agroforestry Systems*, *90*(4), 563–576. https://doi.org/10.1007/s10457-015-9841-7

Tagesson, T, Ardö, J., Cappelaere, B., Kergoat, L., Abdi, A., Horion, S., & Fensholt, R. (2017). Modelling spatial and temporal dynamics of gross primary production in the Sahel from earth-observation-based photosynthetic capacity and quantum efficiency. *Biogeosciences*, *14*(5), 1333–1348. https://doi.org/10.5194/bg-14-1333-2017

Tagesson, Torbern, Tian, F., Schurgers, G., Horion, S., Scholes, R., Ahlström, A., et al. (2021). A physiology-based Earth observation model indicates stagnation in the global gross primary production during recent decades. *Global Change Biology*, *27*(4), 836–854. https://doi.org/10.1111/gcb.15424

Tsuruta, A., Aalto, T., Backman, L., Hakkarainen, J., Van Der Laan-Luijkx, I. T., Krol, M. C., et al. (2017). Global methane emission estimates for 2000-2012 from CarbonTracker Europe-CH4 v1.0. *Geoscientific Model Development*, *10*(3), 1261–1289. https://doi.org/10.5194/gmd-10-1261-2017

UNEP (2022). *Global Peatlands Assessment – The State of the World's Peatlands: Evidence for action toward the conservation, restoration, and sustainable management of peatlands.* Main Report. Global Peatlands Initiative. United Nations Environment Programme, Nairobi.

United Nations Urban Settlement Programme. (2019). *World population prospects 2019. Department of Economic and Social Affairs. World Population Prospects 2019.*

Valentini, R., Arneth, A., Bombelli, A., Castaldi, S., Gatti, R. C., Chevallier, F., et al. (2014). A full greenhouse gases budget of africa: Synthesis, uncertainties, and vulnerabilities. *Biogeosciences*, *11*(2), 381–407. https://doi.org/10.5194/bg-11-381-2014

Van Der Laan-Luijkx, I. T., Van Der Velde, I. R., Van Der Veen, E., Tsuruta, A., Stanislawska, K., Babenhauserheide, A., et al. (2017). The CarbonTracker Data Assimilation Shell (CTDAS) v1.0: Implementation and global carbon balance 2001-2015. *Geoscientific Model Development*, *10*(7), 2785–2800. https://doi.org/10.5194/gmd-10-2785-2017

Van Der Werf, G. R., Randerson, J. T., Giglio, L., Van Leeuwen, T. T., Chen, Y., Rogers, B. M., et al. (2017). Global fire emissions estimates during 1997-2016. *Earth System Science Data*, *9*(2), 697–720. https://doi.org/10.5194/essd-9-697-2017

Venter, Z. S., Cramer, M. D., & Hawkins, H.-J. (2018). Drivers of woody plant encroachment over Africa. *Nature Communications*, *9*(1), 2272. https://doi.org/10.1038/s41467-018-04616-8

Wang, F., Maksyutov, S., Tsuruta, A., Janardanan, R., Ito, A., Sasakawa, M., et al. (2019). Methane emission estimates by the global high-resolution inverse model using national inventories. *Remote Sensing*, *11*(21), 1–19. https://doi.org/10.3390/rs11212489

Wang, M., Wigneron, J. P., Sun, R., Fan, L., Frappart, F., Tao, S., et al. (2021). A consistent record of vegetation optical depth retrieved from the AMSR-E and AMSR2 X-band observations. *International Journal of Applied Earth Observation and Geoinformation*, *105*. https://doi.org/10.1016/j.jag.2021.102609

Wang, S., Zhang, Y., Ju, W., Chen, J. M., Ciais, P., Cescatti, A., et al. (2020). Recent global decline of CO_2 fertilization effects on vegetation photosynthesis. *Science*, *370*(6522), 1295–1300. https://doi.org/10.1126/science.abb7772

Williams, C. A., Hanan, N. P., Neff, J. C., Scholes, R. J., Berry, J. A., Denning, A. S., & Baker, D. F. (2007a). Africa and the global carbon cycle. *Carbon Balance and Management*, *2*(1), 3. https://doi.org/10.1186/1750-0680-2-3

Williams, C. A., Hanan, N. P., Neff, J. C., Scholes, R. J., Berry, J. A., Denning, A. S., & Baker, D. F. (2007b). Africa and the global carbon cycle. *Carbon Balance and Management*, *2*(1), 3. https://doi.org/10.1186/1750-0680-2-3

Winkler, A. J., Myneni, R. B., Hannart, A., Sitch, S., Haverd, V., Lombardozzi, D., et al. (2021). Slowdown of the greening trend in natural vegetation with further rise in atmospheric CO2. *Biogeosciences*, *18*(17), 4985–5010. https://doi.org/10.5194/bg-18-4985-2021

White, Frank; 1983; Vegetation of Africa - a descriptive memoir to accompany the Unesco/AETFAT/UNSO vegetation map of Africa; Natural Resources Research Report XX; U. N. Educational, Scientific and Cultural Organization; 7 Place de Fontenoy, 75700 Paris, France; 356 pages.

Wolf, J., Asrar, G. R., & West, T. O. (2017). Revised methane emissions factors and spatially distributed annual carbon fluxes for global livestock. *Carbon Balance and Management*, *12*(1). https://doi.org/10.1186/s13021-017-0084-y

Yuan, W., Zheng, Y., Piao, S., Ciais, P., Lombardozzi, D., Wang, Y., et al. (2019). Increased atmospheric vapor pressure deficit reduces global vegetation growth. *Science Advances*, *5*(8), eaax1396. https://doi.org/10.1126/sciadv.aax1396

Zhao, Z., Li, W., Ciais, P., & Wigneron, J.-P. (2022). Central African Biomass Carbon Loss Counterbalanced by Carbon Gains during 2010-2019. In *AGU Fall Meeting Abstracts* (Vol. 2022, pp. B51D-03).

Zheng, B., Ciais, P., Chevallier, F., Chuvieco, E., Chen, Y., & Yang, H. (2021). Increasing forest fire emissions despite the decline in global burned area. *Science Advances*, *7*(39), eabh2646. https://doi.org/10.1126/sciadv.abh2646

Zhou, Y., Staver, A. C., & Davies, A. B. (2023). Species-level termite methane production rates. *Ecology*, *104*(2), e3905. https://doi.org/10.1002/ecy.3905

Zscheischler, J., Mahecha, M. D., Avitabile, V., Calle, L., Carvalhais, N., Ciais, P., et al. (2017). Reviews and syntheses: An empirical spatiotemporal description of the global surface-atmosphere carbon fluxes: Opportunities and data limitations. *Biogeosciences*, *14*(15), 3685–3703. https://doi.org/10.5194/bg-14-3685-2017

Zubkova, M., Boschetti, L., Abatzoglou, J. T., & Giglio, L. (2019). Changes in fire activity in Africa from 2002 to 2016 and their potential drivers. *Geophysical Research Letters*, *46*(13), 7643–7653.